Short article

Molecular Cell

Oncogene-dependent *sloppiness* in mRNA translation

Graphical abstract

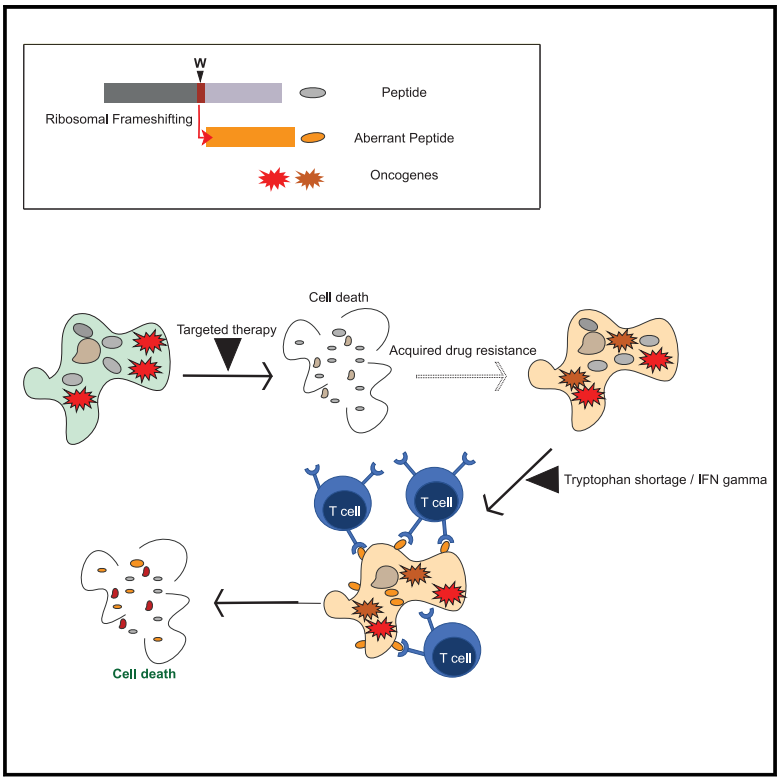

Authors

Julien Champagne, Abhijeet Pataskar, Naomi Blommaert, ..., Daniel S. Peeper, William J. Faller, Reuven Agami

Correspondence

r.agami@nki.nl

In brief

When amino acids are scarce, cancer cells are prone to produce aberrant protein. Here, Champagne et al. show that these errors result from the hyperactivation of oncogenic pathways. This cancer behavior represents a therapeutic opportunity by allowing T lymphocytes to recognize and kill resistant tumors.

Highlights

- *Sloppiness* is defined by ribosomal frameshifting upon tryptophan shortage
- MAPK pathway hyperactivation links *sloppiness* to cancer
- *Sloppiness* causes aberrant peptide presentation at the cell surface
- Drug-resistant cancer cells remain sloppy and are targeted by T cells

Champagne et al., 2021, Molecular Cell *81*, 4709–4721
November 18, 2021
https://doi.org/10.1016/j.molcel.2021.09.002

CellPress

Molecular Cell

CellPress
OPEN ACCESS

Short article

Oncogene-dependent *sloppiness* in mRNA translation

Julien Champagne,[1,7] Abhijeet Pataskar,[1,7] Naomi Blommaert,[1] Remco Nagel,[1] Demi Wernaart,[1] Sofia Ramalho,[1] Juliana Kenski,[5] Onno B. Bleijerveld,[2] Esther A. Zaal,[3,4] Celia R. Berkers,[3,4] Maarten Altelaar,[2,4] Daniel S. Peeper,[5] William J. Faller,[1] and Reuven Agami[1,6,8,*]

[1]Division of Oncogenomics, Oncode Institute, the Netherlands Cancer Institute, Plesmanlaan 121, 1066CX Amsterdam, the Netherlands
[2]Proteomics Facility, The Netherlands Cancer Institute, Plesmanlaan 121, 1066CX Amsterdam, the Netherlands
[3]Department of Biochemistry and Cell Biology, Faculty of Veterinary Medicine, Utrecht University, Utrecht, the Netherlands
[4]Biomolecular Mass Spectrometry and Proteomics, Bijvoet Center for Biomolecular Research, Utrecht Institute for Pharmaceutical Sciences, Utrecht University and Netherlands Proteomics Centre, Utrecht, the Netherlands
[5]Division of Molecular Oncology & Immunology, Oncode Institute, The Netherlands Cancer Institute, Plesmanlaan 121, 1066CX Amsterdam, the Netherlands
[6]Erasmus MC, Rotterdam University, Rotterdam, the Netherlands
[7]These authors contributed equally
[8]Lead contact
*Correspondence: r.agami@nki.nl
https://doi.org/10.1016/j.molcel.2021.09.002

SUMMARY

mRNA translation is a highly conserved and tightly controlled mechanism for protein synthesis. Despite protein quality control mechanisms, amino acid shortage in melanoma induces aberrant proteins by ribosomal frameshifting. The extent and the underlying mechanisms related to this phenomenon are yet unknown. Here, we show that tryptophan depletion-induced ribosomal frameshifting is a widespread phenomenon in cancer. We termed this event *sloppiness* and strikingly observed its association with MAPK pathway hyperactivation. *Sloppiness* is stimulated by RAS activation in primary cells, suppressed by pharmacological inhibition of the oncogenic MAPK pathway in sloppy cells, and restored in cells with acquired resistance to MAPK pathway inhibition. Interestingly, *sloppiness* causes aberrant peptide presentation at the cell surface, allowing recognition and specific killing of drug-resistant cancer cells by T lymphocytes. Thus, while oncogenes empower cancer progression and aggressiveness, they also expose a vulnerability by provoking the production of aberrant peptides through *sloppiness*.

INTRODUCTION

Eukaryotic mRNA translation is a highly regulated and conserved mechanism (Tuller et al., 2010; Jackson et al., 2010). Recent publications highlighted a connection between translation efficiency and the transformed phenotype required for tumor initiation, growth, and metastasis. Most prominent among these links are oncogenic pathways such as the RAS-mitogen-activated protein kinase (MAPK), mammalian target of rapamycin (mTOR), YAP1, and Myc (Bhat et al., 2015; Truitt and Ruggero, 2017; Barna et al., 2008). These oncogenic signaling pathways stimulate mRNA translation initiation via the eIF4F (eukaryotic initiation factor 4F) protein complex (Pelletier et al., 2015; Waskiewicz et al., 1999; Ma and Blenis, 2009; Pyronnet et al., 1999). Overexpression of eIF4E, a rate-limiting factor of the eIF4F complex, was found to be sufficient to induce spontaneous lymphomagenesis in mice (Ruggero et al., 2004). Moreover, haplo-insufficient levels of eIF4E abrogate tumor formation without affecting normal tissue development in mice (Truitt et al., 2015). In addition, eIF4E regulates the mTOR complex 1 (mTORC1), an essential factor in cancer initiation and metastasis that functions by phosphorylating the p70S6 kinase (S6K) and the eukaryotic translation initiation factor 4E binding protein 1 (eIF4EBP1), respectively positive and negative regulators of mRNA translation (Aoki et al., 2001; Hsieh et al., 2010, 2012). In addition to oncogenic signaling, ribosome concentration and tRNA modifications were shown to play key roles in cancer cell behavior. For example, high expression of the ribosomal protein RPL15 in circulating tumor cells increased their metastatic capacity (Ebright et al., 2020), and a tRNA modification at uridine 34 (U34) was described to promote melanoma cell survival (Rapino et al., 2018). This evidence pinpoints the causative role of deregulating mRNA translation in cancer development and indicates the central role of oncogenes in this effect.

The central role of active RAS-MAPK and PI3K (phosphatidylinositol 3-kinase)-AKT-mTOR pathways in oncogenesis is exemplified by experiments using numerous small-molecule inhibitors to target crucial members of these axes (Bhat et al., 2015). On the one hand, inhibitors that target RAS, RAF, MEK, or MNK prevent eIF4F complex initiation (Pelletier et al., 2015; Malka-Mahieu et al., 2017). On the other hand, compounds that effectively inhibit mTORC1 and mTORC2 suppress protein

synthesis by inhibiting the phosphorylation of key regulators of mRNA translation and ribosome synthesis (Hua et al., 2019; Liu and Sabatini, 2020). However, despite the effective inhibition of BRAF (e.g., vemurafenib), MEK1/2 (trametinib), and mTORC1 (everolimus) that can lead to initial disease control, the majority of patients acquire resistance to these treatments (Wagle et al., 2014; Di Nicolantonio et al., 2010).

Interestingly, resistance to everolimus was associated with oncogenic mutations in KRAS, indicating a link between oncogenic RAS and the mTOR pathway (Di Nicolantonio et al., 2010). Both pathways influence protein synthesis by regulating the activity of the ribosomal subunit S6 (RPS6). RPS6 is a component of the 40-s ribosomal subunit with 5 serine residues located at its C-terminal part that are phosphorylated to ensure its functions (Krieg et al., 1988). Published reports indicate that p90S6 kinases (RPS6KA1–4), regulated by the RAS-RAF-MEK-ERK pathway, and the p70S6 kinases (RPS6KB1–2), regulated by the PI3K-mTOR pathway, are responsible for RPS6 phosphorylation (Roux et al., 2007; Fingar and Blenis, 2004). Interestingly, hyperphosphorylation of RPS6 predicts unfavorable clinical survival in lung cancer (Chen et al., 2015). In line with this notion, targeting RPS6KB1 prevented metastasis in a mice model (Akar et al., 2010). These findings indicate the significance of deregulating protein synthesis for oncogenic function in cancer development and progression.

To ensure an efficient protein synthesis, quality control surveillance mechanisms sense the state of mRNA translation to resolve emerging problems. In particular, the ribosome-mediated quality control complex (RQC), which senses stalled ribosomes to induce ribosome subunits splitting and nascent peptide degradation, is a highly conserved mechanism from yeast to human (Brandman and Hegde, 2016). Another layer of control mechanism for protein synthesis is made by sensing amino acid levels. The General Control Nonderepressible 2 (GCN2/EIF2AK4)-ATF4 pathway senses uncharged tRNA and consequently reduces mRNA translation initiation and elongation via mTOR and eIF2α (Ishimura et al., 2016). In addition, this pathway induces the expression of genes such as asparagine synthetase (ASNS) to promote cell survival (Ye et al., 2010). In stress conditions with extensive damage to mRNA, colliding ribosomes are recognized by ZAKα, a kinase that either triggers survival by the GCN2-eIF2α pathway or induces apoptosis via SAPK (p38/JNK) when the level of collided ribosomes is too high (Wu et al., 2020).

Despite control mechanisms of protein synthesis, programmed ribosomal frameshifting (PRF) can occur during the mRNA translation of certain viruses and a few cellular genes (Dinman, 2012; Fang et al., 2012; Ivanov and Atkins, 2007). PRF is used to downregulate gene expression by introducing premature translation termination and nonsense-mediated mRNA decay, and to enrich protein diversity by generating alternative protein products (Baranov et al., 2011; Meydan et al., 2017; Penn et al., 2020; Shigemoto et al., 2001). During frameshifting, ribosomes move backward or forward on the mRNA to resume translation in another reading frame (Farabaugh, 1996; Yan et al., 2015). "Slippery" sequences and secondary structures in mRNA were shown to induce ribosomal frameshifting events in certain viruses and few human genes (Dever et al., 2018; Smith et al., 2019; Ketteler, 2012; Clark et al., 2007; Okamura et al., 2006). Moreover, the degree of ribosomal frameshifting at viral slippery sequences can be modulated by host genes (Wang et al., 2019). Beyond the mRNA sequence context, amino acid shortages can induce ribosomal frameshifting in bacteria, eukaryotes, and humans (Weiss and Gallant, 1983; Bartok et al., 2021). In particular, the induction of indoleamine 2,3-dioxygenase enzyme (IDO1) by prolonged interferon-gamma (IFN-γ) exposure of melanoma cells, depletes intracellular tryptophan and stimulates ribosomal frameshifting at the "starved" tryptophan codons (Bartok et al., 2021). These frameshifting events generate *trans-frame* chimeric proteins that are processed and presented by human leukocyte antigen class I (HLA-I) molecules at the surface of melanoma cells to be available for recognition by T lymphocytes (Bartok et al., 2021).

Here, we examined the occurrence of ribosomal frameshifting by tryptophan depletion across cancer types and found a widespread capacity to generate aberrant proteins as a consequence. In contrast, ribosomal frameshifting following tryptophan depletion was undetectable in non-transformed human cells. We, therefore, called this phenomenon *sloppiness*, and further linked it to the hyperactivation of the oncogenic RAS-MAPK pathway and to acquired drug resistance mechanisms. Finally, we demonstrate that the aberrant proteins produced by *sloppiness* can be processed and presented for T lymphocytes at the cell surface.

RESULTS

Sloppiness in mRNA translation is a pervasive phenomenon of cancer cells

We recently demonstrated that tryptophan depletion mediated by T cell activation and IFN-γ signaling stimulates in melanoma cells ribosomal frameshifting at sites of tryptophan codons (Bartok et al., 2021). Expanding on this observation, we asked whether the ability to frameshift when amino acids are scarce is limited to melanoma cells or is it a general phenomenon that indicates a sloppy control on mRNA translation. We used two reporter vectors (called here pSloppy) containing either a control in-frame (Frame; pSloppy^{C}; marked #) or an out-of-frame (+1; pSloppy^{FS}; marked &) tryptophan-less turbo-GFP (tGFP) gene downstream of a V5-tagged ATF4$^{(1-63)}$ fragment with a single tryptophan codon at position 93 (A.A 93) from the translation start site (Figure 1A). To assess *sloppy* mRNA translation behavior, we treated MD55A3 cells for 48 h with IFN-γ, followed by an additional 4 h with a proteasome inhibitor (MG-132) to counter the ATF4$^{1-63}$ instability (Bartok et al., 2021; Figure 1B). Immunoblotting analysis with anti-V5 and anti-tGFP antibodies enabled the detection of ribosomal frameshifting at the tryptophan codon through the induced presence of a longer *trans-frame* aberrant protein containing V5-tag and tGFP (V5-ATF4$^{(1-63)}$-tGFP, marked #) (Figure 1C). The frameshifting event was confirmed by the detection of tGFP-tryptic peptides after V5-immunoprecipitation coupled to mass spectrometry analysis (V5-IP-MS) in IFN-γ-treated conditions (Figure 1D). Furthermore, the addition of an IDO1 inhibitor (IDOi) to the IFN-γ treatment negated frameshifting, showing that the IFN-γ-induced tryptophan depletion is causative to frameshifting (Figure 1C). Finally,

CellPress
OPEN ACCESS

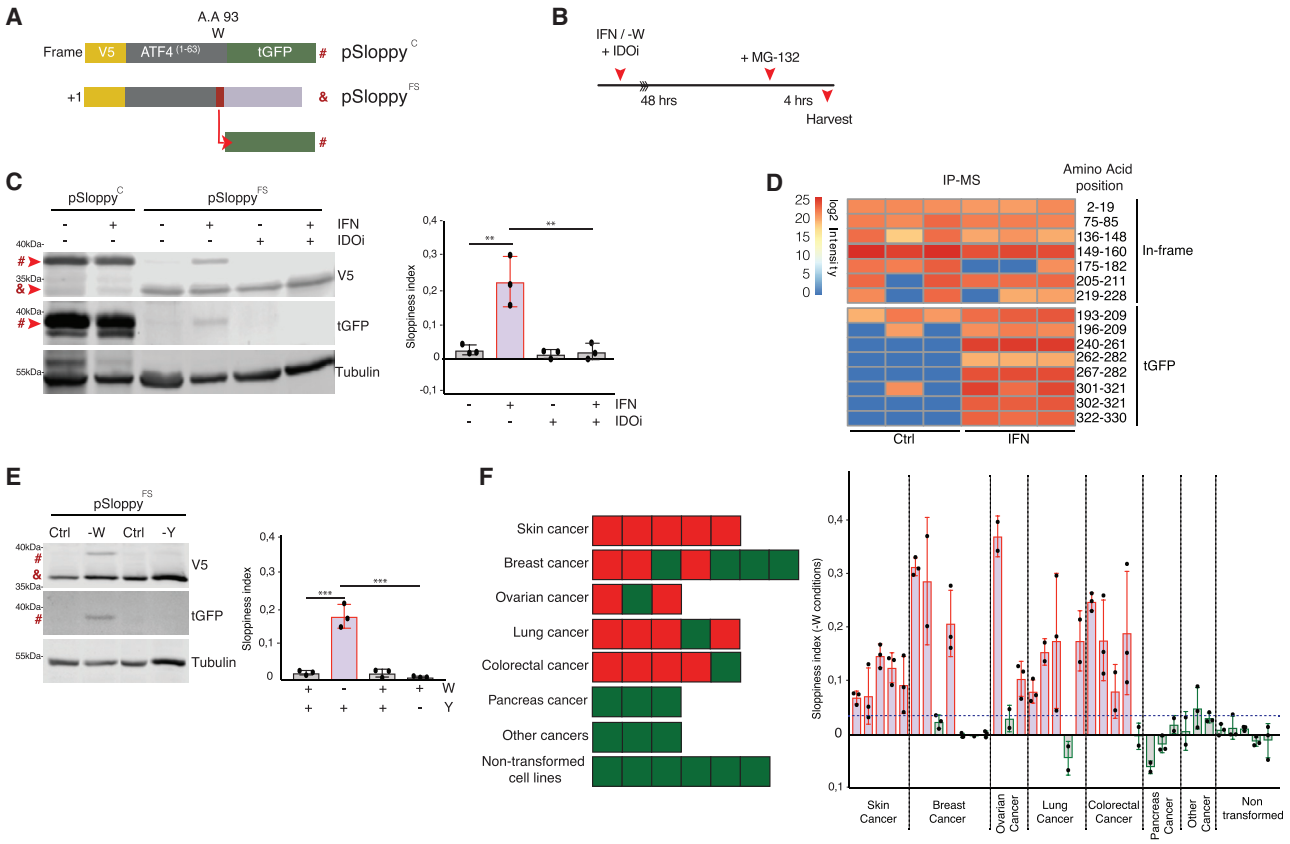

Figure 1. Tryptophan-induced ribosomal frameshifting is a pervasive phenomenon in cancer

(A) Schematic depicting the pSloppy reporter constructs used for the detection of frameshifting events. pSloppy^{C} vector (#): V5-tag (yellow box) fused to the ATF4 gene (ATF4$^{1-63}$, containing 1 tryptophan residue W at amino acid 93 from the translation start site) upstream of tryptophan less-GFP (tGFP, green box); pSloppy^{FS}: 1 additional base pair (red rectangle) after ATF4, leading to an out-of-frame tGFP shorter protein product (&).

(B) Scheme of the experimental pipeline for assessing frameshifting events. Cells were treated with IFN-γ (IFN) or tryptophan-depleted media (-W) for 48 h. Whenever used, IDO1 inhibitor (IDOi) was added at the same time as IFN-γ.

(C) Immunoblot for V5, tGFP, and tubulin of MD55A3 cells expressing pSloppy^{C} or pSloppy^{FS} constructs treated for 48 h with IFN and IDOi, as indicated. A quantification of frameshift efficiency is depicted next to the immunoblot. Values represent the average of the 3 independent experiments ± SD. **p = 0.002, **p = 0.001 by 1-way ANOVA, followed by Bonferroni post hoc test.

(D) Heatmap depicts a bioinformatics analysis of log2 intensities of tryptic in-frame and tGFP peptides of MD55A3 cells expressing the pSloppy^{FS} construct treated for 48 h with IFN-γ and then subjected to anti-V5-immunoprecipitation followed by mass spectrometry (IP-MS). Each column represents an independent technical replicate (n = 3).

(E) Immunoblot for V5, tGFP, and tubulin of MD55A3 expressing pSloppy^{FS} construct treated for 48 h with tryptophan- (-W) or tyrosine- (-Y) depleted medium. The quantification of frameshift efficiency is indicated. Values represent the average of the 3 independent experiments ± SD. ***p < 0.001 by 1-way ANOVA, followed by Bonferroni post hoc test.

(F) Schematic representation of the ribosomal frameshifting capability of various human cancer and untransformed cell lines. Frameshifting ability was assessed by immunoblot analysis using cells containing the pSloppy^{FS} reporter construct that were treated with tryptophan depletion (-W) for 48 h (Figures S1C and S1D). The red symbols represent cells that show a ribosomal frameshifting following tryptophan depletion and the green shows the cell lines that did not demonstrate detectable frameshifting.

the generation of tGFP from this vector by frameshifting was explicitly caused by the shortage of tryptophan, as depleting tyrosine, did not induce *trans-frame* aberrant tGFP protein expression (Figures 1E and S1A).

To examine the prevalence of ribosomal frameshifting following amino acid depletion across cell types, we introduced pSloppy^{C} and pSloppy^{FS} vectors to various cell lines from cancerous and non-cancerous origins, and performed immunoblot analyses to detect the occurrence of aberrant proteins. To avoid inconsistencies between cell lines due to variable IFN-γ-induced IDO1 levels, we directly generated tryptophan shortage using a tryptophan-less medium (Figure S1A). We confirmed signaling by tryptophan depletion in a panel of examined cell lines by measuring the mRNA levels of ASNS, an enzyme activated by the GCN2-ATF4 cascade in response to amino acid shortage (Figure S1B; Siu et al., 2002). As expected, all five examined melanoma cell lines showed frameshifting by tryptophan depletion (Figures 1F and S1C, first lane). More globally, frameshifting was also detected in the majority (18/31) of the tested, colon, lung, ovarian, and breast cancer cell types, albeit to different

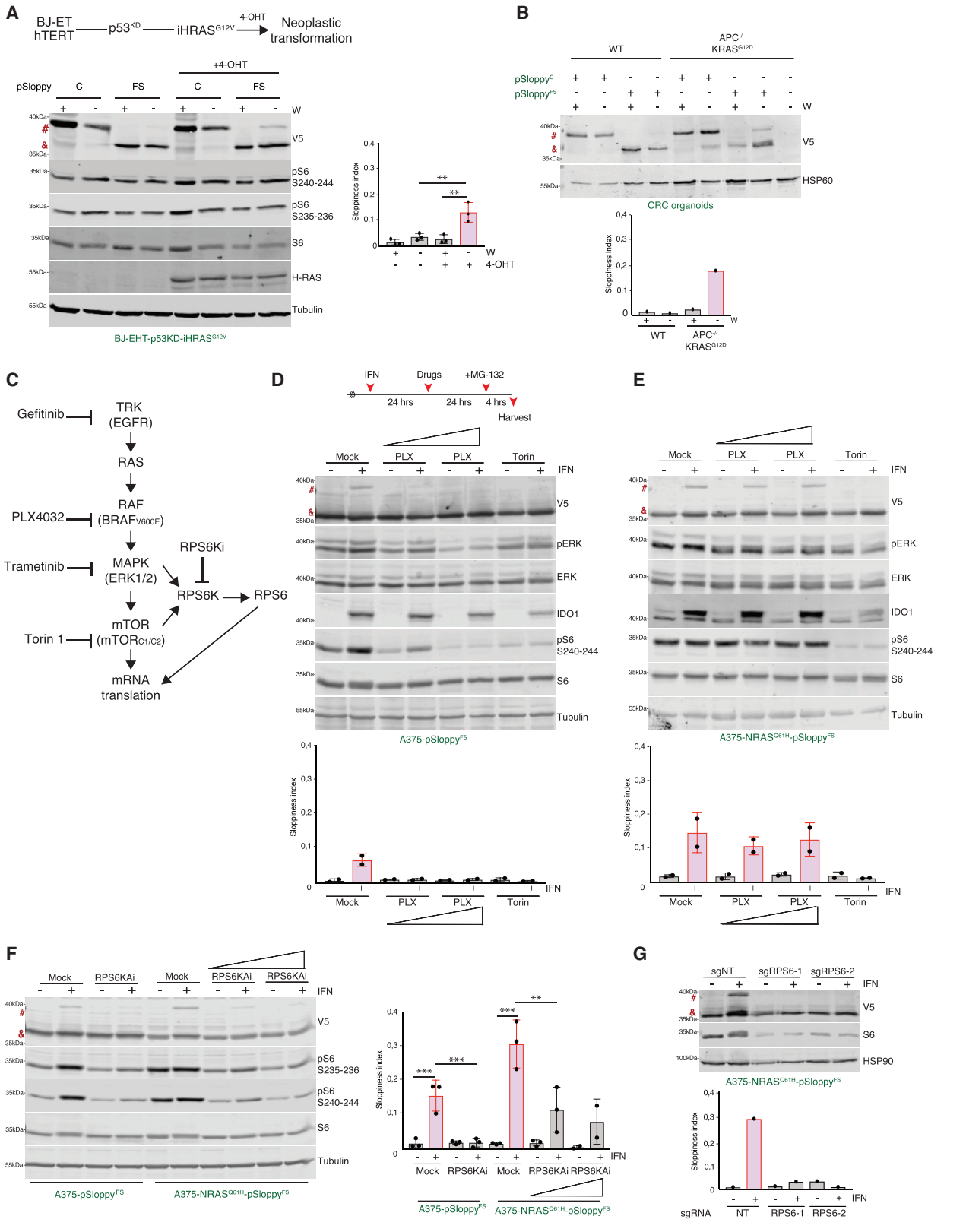

(legend on next page)

extents (Figures 1F and S1C). In sharp contrast, none of the tested non-cancerous cell lines (RPE-1, MCF 10A, BJ, and TIG-3) showed a detectable generation of the tGFP-containing frameshifted product (Figures 1F and S1D). Moreover, tryptophan depletion did not effectively facilitate frameshifting of the non-transformed human embryonic kidney HEK293T cell line, containing the SV40 large T antigen that blocks both the p53 and Rb pathway, suggesting that these two tumor suppressor pathways are not involved in this effect (Figures S1D and S1E). V5-IP-MS assays performed on a selected panel of cell lines expressing pSloppy^{FS} confirmed the immunoblot results (Figure S1F). These results suggest that the induction of frameshifting following tryptophan shortage is a widespread event that can take place in cancer cells. Therefore, we called this phenomenon *sloppiness* in mRNA translation.

Sloppiness is associated with specific cancer-causing genetic alterations

The extensive *sloppiness* observed in cancer prompted us to investigate whether specific cancer-driving somatic aberrations are linked to it. This analysis has indicated that *sloppiness* was neither associated with the loss of p53 activity (11/18 sloppy and 8/13 non-sloppy cancer cell lines had p53 genetic aberrations), nor with pRb loss, as 16/18 sloppy cancer cell lines contained wild-type (WT) pRb alleles (Figures S1D and S1E; Table S1). Instead, a large proportion of the sloppy cell lines had oncogenic mutations associated with the MAPK pathway (including NRAS^{Q61K}, NRAS^{Q61R}, KRAS^{G13D}, KRAS^{G12S}, KRAS^{G12C}, KRAS^{G13D}, KRAS^{G12V}, BRAF^{V600E}, and EGFR$^{Q746\text{-}A750del}$; Table S1). However, the observation that 5 of 13 of the non-sloppy cell lines also had various prominent oncogenic mutations in KRAS (KRAS^{G12C}, KRAS^{G12D}, KRAS^{G12V}) may indicate that MAPK pathway activation may not be sufficient to elicit *sloppiness*, and other factors (e.g., associated somatic mutations, tissue context) are likely to be involved.

Causal involvement of the oncogenic RAS/MAPK pathway in *sloppiness*

To examine a causal link between oncogenic MAPK pathway activation and *sloppiness*, we initially focused on RAS and took advantage of the well-established neoplastic transformation model of human primary BJ fibroblast cells expressing an inducible oncogenic HRAS^{G12V} (Voorhoeve et al., 2006; Figure 2A, scheme). We introduced pSloppy^{FS} and pSloppy^{C} reporters into BJ-ET-p53kd-iHRAS^{G12V} (BJ cells expressing the ecotropic receptor, human telomerase [hTERT], a small hairpin RNA [shRNA] against p53, and a tamoxifen-inducible oncogenic HRAS^{G12V}). These cells were either mock treated or exposed to tamoxifen for 7 days to induce oncogenic HRAS^{G12V} expression (Figure 2A). We controlled for oncogenic RAS expression and its impact on mRNA translation by HRAS immunostaining and RPS6 phosphorylation, as previously observed (Roux et al., 2007). During the last 2 days of RAS induction, we depleted tryptophan for 48 h and harvested cells for immunoblot analyses. Figure 2A shows the detection of *sloppiness* only upon HRAS^{G12V} induction. V5-IP-MS assays performed on these cells confirmed the immunoblot results (Figure S2A). The low level of tGFP peptides found induced by tryptophan depletion in the control cells are likely the result of leakiness of the inducible HRAS^{G12V} system.

Next, we interrogated organoids derived from a genetically engineered mouse model for RAS-induced colorectal cancer. We used organoid cultures from WT and APC$^{-/-}$ KRAS^{G12D} mice (van Es and Clevers, 2015; Sato et al., 2009), introduced pSloppy^{C} and pSloppy^{FS}, and depleted tryptophan, as indicated above (Figure 1B). Remarkably, frameshifting was readily observed in the APC$^{-/-}$ KRAS^{G12D} but not WT organoids (Figure 2B), indicating the conservation of *sloppiness* downstream of oncogenic RAS.

Finally, to further substantiate the link between oncogenic MAPK pathway and *sloppiness*, we used small-molecule inhibitors to suppress this signaling pathway in sloppy cancer cells. We initially monitored *sloppiness* in BRAF^{V600E}-driven A375 melanoma cells treated with either vemurafenib, a potent BRAF^{V600E} inhibitor, or Torin-1, a potent mTORC1/2 inhibitor (Figure 2C). As a control for these treatments, we used an A375-derivative cell line endogenously expressing a mutant NRAS^{Q61H} and displaying acquired resistance to dabrafenib, another BRAF^{V600E} inhibitor (Wang et al., 2018). We initiated tryptophan depletion in A375-pSloppy^{FS} and A375-NRAS^{Q61H}-pSloppy^{FS} cells using

Figure 2. MAPK oncogenic pathway drives *sloppiness* upon tryptophan shortage

(A) Upper panel: a schematic representation of the strategy used to fully transform human fibroblast BJ cells. Main panel: BJ-EHT-p53^{KD}-iHRAS^{G12V} cells, expressing pSloppy^{C} or pSloppy^{FS} constructs, were treated for 4 consecutive days with 4-OHT-tamoxifen (+TMX) to induce HRAS^{G12V}, then were cultured (with TMX) for an additional 48 h in either tryptophan depleted (-) or control (+) media, and immunoblotted for V5, HRAS, pRPS6 (S235–236; S240–244), RPS6, and tubulin. The quantification of frameshifting efficiency is also depicted. Values represent the average of the 3 independent experiments ± SD. **p = 0.005 and **p = 0.003 by 1-way ANOVA, followed by Bonferroni post hoc test.

(B) Immunoblot analysis for V5 and HSP60 of WT or APC$^{-/-}$ KRAS^{G12D} colorectal cancer (CRC) organoids expressing pSloppy^{C} or pSloppy^{FS} constructs. CRC organoids were cultured in the presence or absence of tryptophan (W) for 48 h before harvesting.

(C) Scheme representing the link between the MAPK pathway and the mTOR pathway. The scheme also represents the inhibitors used in the rest of the study.

(D) Upper panel: a schematic representation of the experimental pipeline for assessing the effects of the drug on frameshifting events. Cells were treated with IFN-γ (IFN) for 48 h. Drugs were added to the medium 24 h after the start of the experiment. Main panel: immunoblot analysis of V5, pERK, ERK, IDO1, pRPS6 (S240–244), RPS6, and tubulin from A375 cells expressing pSloppy^{FS} treated as indicated. PLX4032 (PLX, 50 nM, 500 nM) and Torin-1 (Torin, 250 nM). Frameshifting efficiency is depicted below the Western blot. Values represent the average of 2 independent experiments ± SD.

(E) Similar to panel D, except that A375-NRAS^{Q61H} cells expressing pSloppy^{FS} were used.

(F) Immunoblot for V5, pRPS6 (S235–236), pRPS6 (S240–244), RPS6, and tubulin of A375-pSloppy^{FS} and A375-NRAS^{Q61H}-pSloppy^{FS} treated for 48 h with IFN-γ (IFN). After 24 h, cells were also treated with RPS6KA1-3 inhibitor (RPS6KAi; 10 μM, 20 μM). The quantification of frameshifting efficiency is also displayed. Values represent the average of the 3 independent experiments ± SD. **p = 0.007 and ***p < 0.001 by 1-way ANOVA, followed by Bonferroni post hoc test.

(G) Immunoblot for V5, RPS6, and HSP-90 of A375-NRAS^{Q61H}-pSloppy^{FS} knocked out by CRISPR-Cas9 for RPS6 (2 independent sgRPS6s) or expressing a control single-guide RNA (sgNT) and treated for 48 h with IFN-γ (IFN). Quantification of frameshifting efficiency is depicted below.

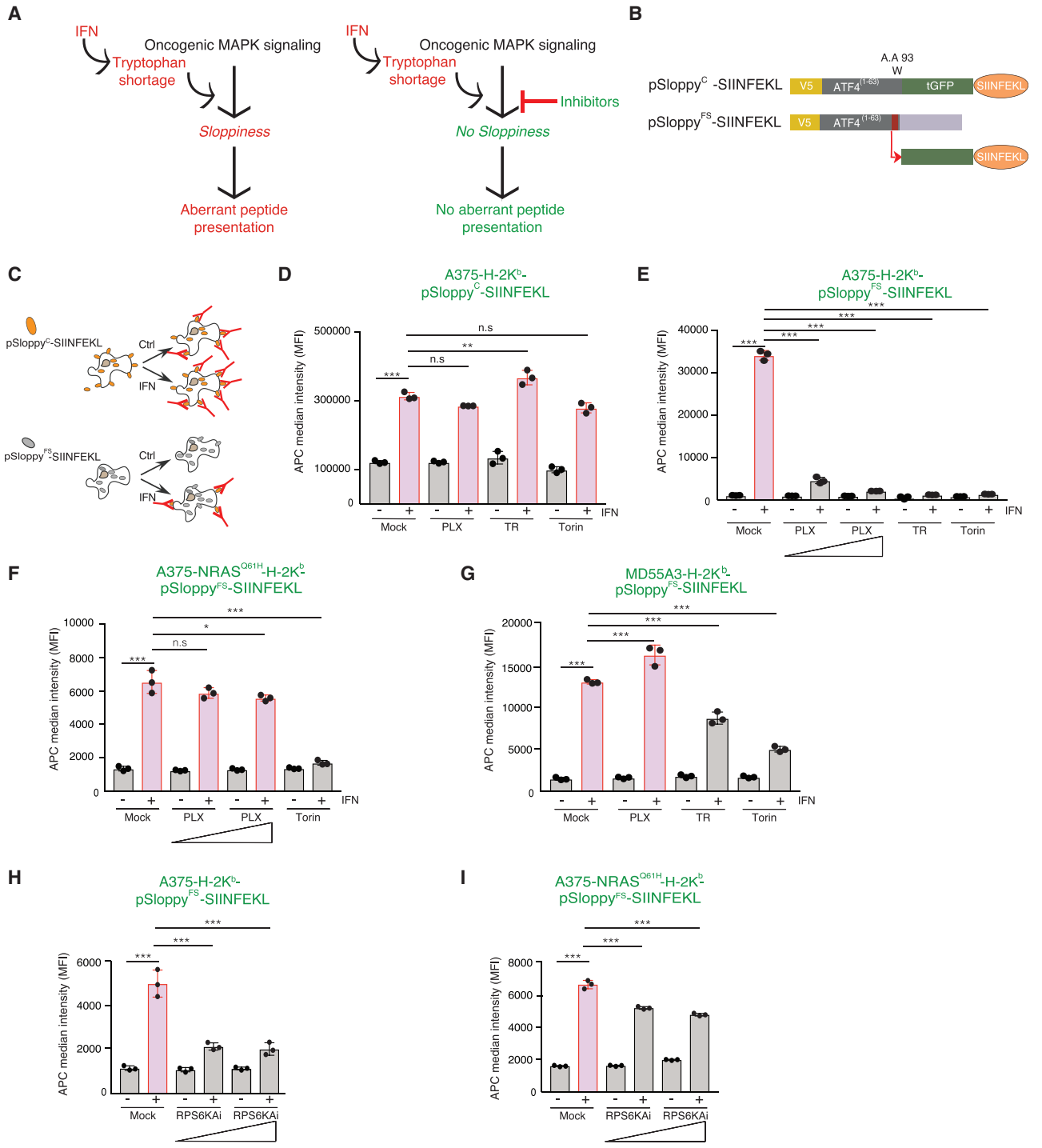

Figure 3. Suppression of oncogenic RAS/MAPK signaling inhibits aberrant peptide presentation upon tryptophan shortage

(A) Left: a scheme of the effect of IFN-γ-mediated tryptophan shortage on *sloppiness* and aberrant peptide presentation in cells containing oncogenic MAPK signaling. Right: inhibitors that were shown to suppress *sloppiness* are predicted to inhibit the presentation of aberrant peptides.

(B) Schematic of the reporter constructs used for detection of the presentation of aberrant peptides. The constructs are the same as presented in Figure 1A, with the addition of the SIINFEKL sequence at the C-terminal part (orange circle).

(C) A scheme representing the recognition of SIINFEKL by 25-D1.16 antibody directed against an H-2K^b-bound-SIINFEKL at the cell membrane. Cells expressing the pSloppy^C-SIINFEKL are recognized in all conditions by the SIINFEKL antibody (red). In cells expressing pSloppy^{FS}-SIINFEKL, SIINFEKL is not displayed at the membrane in normal conditions. Upon IFN-γ-mediated tryptophan depletion, ribosomal frameshifting events at the tryptophan codon are expected to lead to SIINFEKL expression, processing, and presentation (lower panel).

(legend continued on next page)

IFN-γ for 24 h, then added the 2 drugs on top of IFN-γ for an additional 24-h treatment (Figure 2D, scheme). In line with the role of oncogenic MAPK pathway activation in the induction of *sloppiness*, frameshifted products were readily induced by IFN-γ in both cell lines (Figures 2D and 2E). However, while vemurafenib suppressed *sloppiness* in WT A375 cells at a concentration as low as 50 nM, the addition of up to 500 nM vemurafenib did not suppress ribosomal frameshifting in A375-NRAS^{Q61H} (PLX; Figures 2D and 2E). Torin-1, in contrast, suppressed *sloppiness* in both cell lines (Figures 2D and 2E), indicating a role of mTOR pathway downstream of oncogenic MAPK signaling, and the specificity of the induced *sloppiness* in mRNA translation. The loss of *sloppiness* in A375 cells was associated with reduced phosphorylation of RPS6, a prominent substrate of RPS6KA and RPS6KB kinases from the mTOR and RAS-MAPK pathways (Figure 2D; Jefferies et al., 1997). In contrast, in A375-NRAS^{Q61H}, phosphorylation of RPS6 was not affected by vemurafenib treatment (Figure 2E), highlighting the central contribution of the RAS-MAPK pathway in *sloppiness* induction.

As additional controls for specificity, we treated the sloppy BRAF^{V600E}-driven HT-29, A375, and SK-MEL-28 colorectal and melanoma cancer cells, respectively, and the sloppy NRAS^{Q61R}-driven MD55A3 melanoma cell line, with vemurafenib (PLX) and observed explicit suppression of *sloppiness* in HT29, A375, and SKMEL-28, but not in MD55A3, upon tryptophan depletion (Figures S2B–S2F). As expected, Torin-1 prevented *sloppiness* in all of the cell lines (Figures S2B–S2F). Furthermore, similar to Torin-1, the inhibition of MEK1/2, upstream of ERK and downstream of BRAF, by trametinib suppressed *sloppiness* in the four cell lines (Figures S2B–S2F). Once more, *sloppiness* appeared to be linked to the phosphorylation status of RPS6 (Figures S2B–S2E). To confirm the specific involvement of the MAPK pathway in *sloppiness* and to control for possible cell-cycle and/or toxic effects, we treated A375 cells with either nocodazole (a mitotic progression inhibitor) or nutlin-3 (activator of the p53 pathway). These drugs did not reduce *sloppiness* efficiency when combined with tryptophan depletion (Figure S2G). Lastly, gefitinib (GEF, an inhibitor of oncogenic epidermal growth factor receptor [EGFR], a tyrosine kinase receptor upstream of RAS) impeded ribosomal frameshifting in HCC827, a non-small cell lung cancer (NSCLC) cell line with an activating EGFR deletion (E746-A750) (Figures S2H and S2I). GEF treatment was specific to HCC827 as the *sloppiness* of other cancer cell lines expressing BRAF^{V600E} or NRAS^{Q61R} was not affected by this drug (Figures S2B–S2F). As expected, the *sloppiness* in HCC827 was also suppressed by Torin-1, but not by vemurafenib or trametinib (Figure S2H). Here, too, *sloppiness* was associated with RPS6 phosphorylation (Figure S2H). The close association of *sloppiness* with RPS6 phosphorylation in MAPK pathway mutated cell lines prompted us to examine it in cells treated with LJH685, a specific inhibitor of RPS6KA1-3 (RPS6KAi; Moyano-Galceran et al., 2020; Kosnopfel et al., 2017). As predicted, RPS6KAi treatment suppressed *sloppiness* in A375 as well as in the NRAS^{Q61H} resistant cells (Figure 2F). We substantiated this result by demonstrating loss of *sloppiness* in cells with RPS6 CRISPR-Cas9 knockouts (Figure 2G). These results strongly indicate that a potent oncogenic activation of the MAPK signaling pathway induces ribosomal frameshifting when tryptophan is limiting via the constitutive activation of mTOR and the phosphorylation of RPS6.

Sloppiness-induced presentation of aberrant peptides requires oncogenic MAPK activity

Aberrant proteins can be processed to aberrant peptides that are presented on the cell surface of melanoma cells (Bartok et al., 2021). Therefore, we investigated whether blocking the oncogenic MAPK pathway impairs the presentation of aberrant peptides (Figure 3A). As a model system for this experiment, we used the ovalbumin-derived SIINFEKL peptide and placed it downstream of tGFP in the pSloppy vectors (pSloppy$^{C\text{-}SIINFEKL}$ and pSloppy$^{FS\text{-}SIINFEKL}$; Figure 3B) (Dersh et al., 2019). SIINFEKL is bound by the H-2K^b class 1 MHC molecule, and this complex is recognized by the 25-D1.16 antibody. In basal conditions, we expected that pSloppy$^{FS\text{-}SIINFEKL}$ will not produce detectable SIINFEKL peptides at the plasma membrane, in contrast to pSloppy$^{C\text{-}SIINFEKL}$ (Figure 3C). We also expected that SIINFEKL presentation will be stimulated in pSloppy$^{FS\text{-}SIINFEKL}$ by IFN-γ-mediated tryptophan depletion due to ribosomal frameshifting (Figure 3C). The introduction of pSloppy$^{C\text{-}SIINFEKL}$ to A375-H-2K^b cells resulted in effective cell recognition by the 25-D1.16 antibody, which was moderately upregulated (3-fold) by IFN-γ, likely due to the increased expression of the immunoproteasome, as previously observed (Bartok et al., 2021; Goldberg et al., 2002; McCarthy and Weinberg, 2015; Figure 3D). In

(D) A bar plot depicting the median APC fluorescence intensity (median fluorescence intensity [MFI]) of H2-K^b-bound SIINFEKL peptides in A375-H-2K^b cells expressing pSloppy^{C}-SIINFEKL construct. Cells were treated with IFN-γ for 48 h, and for the last 24 h with the indicated drugs: PLX4032 (PLX, 50 nM), trametinib (TR, 2 nM) and Torin-1 (Torin, 250 nM). Values represent the average of the 3 independent experiments ± SD. **p < 0.01, ***p < 0.001 by 1-way ANOVA, followed by Bonferroni post hoc test.

(E) Similar to (D), except that A375-H-2K^b cells expressing pSloppy^{FS}-SIINFEKL were used. PLX4032 (PLX, 50 nM, 500 nM), trametinib (TR, 2 nM) and Torin-1 (Torin, 250 nM). Values represent the average of the 3 independent experiments ± SD. ***p < 0.001 by 1-way ANOVA, followed by Bonferroni post hoc test.

(F) Bar plot depicting the median APC fluorescence intensity (MFI) of H2-K^b-bound SIINFEKL peptides in A375-NRAS^{Q61H}-H-2K^b cells expressing pSloppy^{FS}-SIINFEKL construct. Cells were treated with IFN-γ for 48 h, and for the last 24 h with the indicated drugs: PLX4032 (PLX, 500 nM, 2,000 nM) and Torin-1 (Torin, 250 nM). Values represent the average of the 3 independent experiments ± SD. *p < 0.05, ***p < 0.001 by 1-way ANOVA, followed by Bonferroni post hoc test.

(G) Similar to (F), except that MD55A3-H-2K^b cells expressing pSloppy^{FS}-SIINFEKL were used. PLX4032 (PLX, 50 nM), trametinib (TR, 2 nM) and Torin-1 (Torin, 250 nM). Values represent the average of the 3 independent experiments ± SD. ***p < 0.001 by 1-way ANOVA, followed by Bonferroni post hoc test.

(H) Bar plot depicting the median APC fluorescence intensity (MFI) of H2-K^b-bound SIINFEKL peptides in A375-H-2K^b cells expressing pSloppy^{FS}-SIINFEKL construct. Cells were treated with IFN-γ for 48 h, and for the last 24 h with LJH685 (RPS6KAi, 5 μM, 10 μM). Values represent the average of the 3 independent experiments ± SD. ***p < 0.001 by 1-way ANOVA, followed by Bonferroni post hoc test.

(I) Similar to (H), except that A375-NRAS^{Q61H}-H-2K^b cells expressing pSloppy^{FS}-SIINFEKL were used. (RPS6KAi, 10 μM, 20 μM). Values represent the average of the 3 independent experiments ± SD. ***p < 0.001 by 1-way ANOVA, followed by Bonferroni post hoc test.

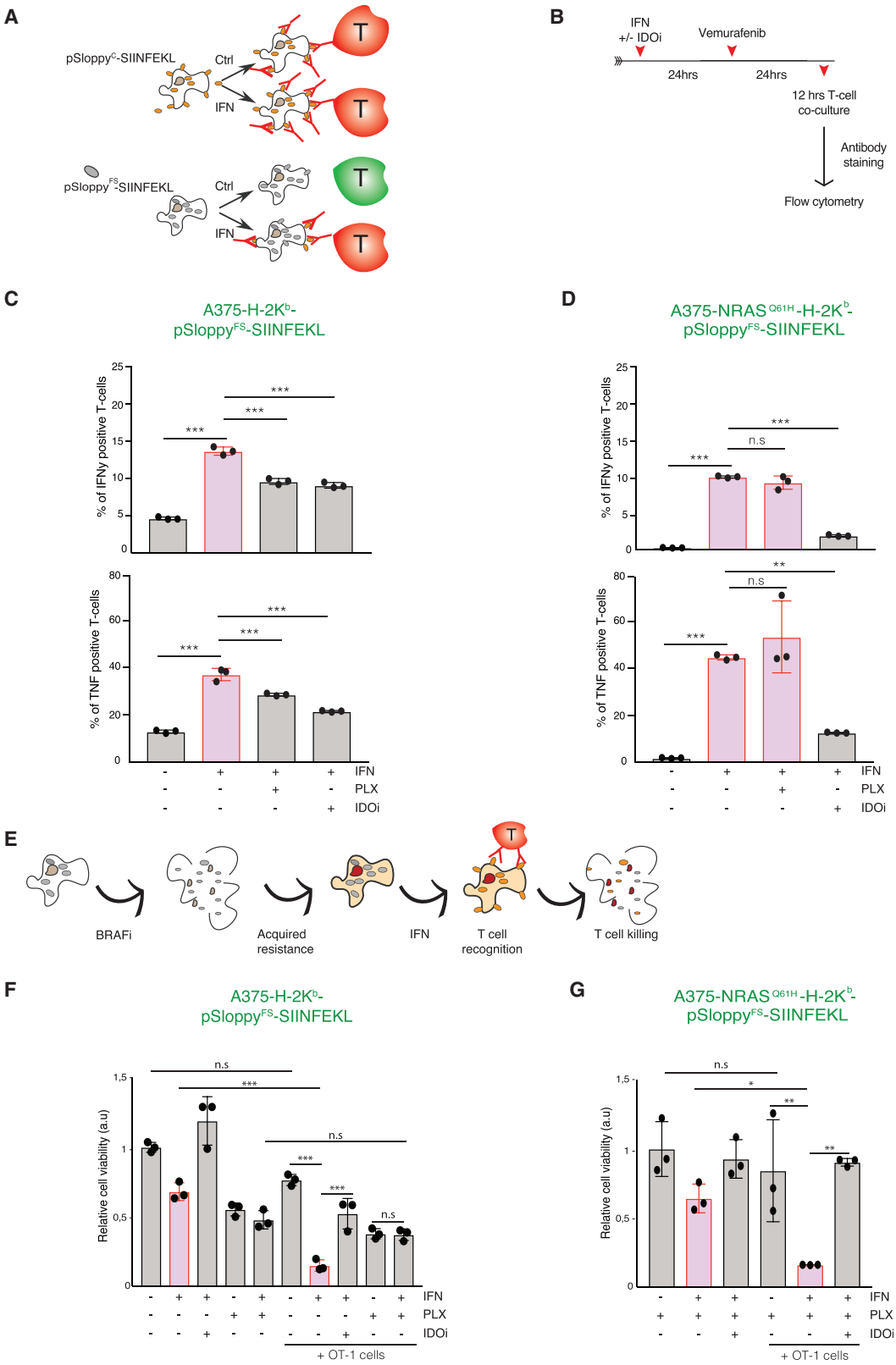

(legend on next page)

contrast, no signal was detected in mock-treated A375-H-2K^b-pSloppy$^{FS\text{-}SIINFEKL}$ cells, while IFN-γ treatment markedly stimulated the recognition of these cells by 25-D1.16, indicating the induced production and presentation of SIINFEKL at the surface of these treated cells (Figure 3E). Interestingly, this stimulation of SIINFEKL presentation by IFN-γ was blocked entirely by either vemurafenib (PLX), trametinib (TR), or Torin-1 (Figure 3E), recapitulating their impact on *sloppiness* in this cell line (Figures 2D, S2C, and S2F). These drugs had no significant effect on the presentation of SIINFEKL in the control in-frame pSloppy$^{C\text{-}SIINFEKL}$ (Figure 3D). In contrast to these MAPK inhibitors, treatment with nocodazole had no significant effect on the induction of SIINFEKL presentation generated by IFN-γ in A375-H-2K^b-pSloppy$^{FS\text{-}SIINFEKL}$ cells compared to either vemurafenib or IDO1 inhibitor (Figure S3A), which is in line with previous observations (Figure S2G).

Next, we examined A375-NRAS^{Q61H}-H-2K^b-pSloppy$^{FS\text{-}SIINFEKL}$ cells and found that they continue to induce SIINFEKL presentation following IFN-γ treatment even at high concentrations (2 μM) of vemurafenib (Figure 3F). In contrast, Torin-1 treatment blocked IFN-γ-induced SIINFEKL presentation without considerably affecting SIINFEKL presentation from pSloppy$^{C\text{-}SIINFEKL}$ (Figures 3F and S3B). These results are consistent with the acquired resistance pattern and the *sloppiness* phenotype of A375-NRAS^{Q61H} cells (Figure 2E). Similar results were also obtained with a different vemurafenib resistant A375-pSloppy$^{FS\text{-}SIINFEKL}$ cell line that expresses an activated version of YAP1 (Hugo et al., 2015; Lin et al., 2015; Figure S3C). Moreover, we used MD55A3-H-2K^b-pSloppy$^{FS\text{-}SIINFEKL}$ melanoma cells (containing NRAS^{Q61R}) to confirm the above results. Here, IFN-γ-mediated induction of SIINFEKL presentation was suppressed by IDO1 inhibition and Torin-1, but not by vemurafenib, as expected from the lack of BRAF mutations in these cells (Figures 3G and S3D). Finally, we confirmed the central role of RPS6 phosphorylation using RPS6KAi, which suppressed SIINFEKL presentation in IFN-γ-treated A375-pSloppy$^{FS\text{-}SIINFEKL}$ cells, and reduced the presentation in A375-NRAS^{Q61H}-pSloppy$^{FS\text{-}SIINFEKL}$, as suggested previously (Figures 2F, 3H, and 3I). These results reinforce the connection between a hyperactive MAPK pathway and *sloppiness*.

Exploiting *sloppiness* for drug-resistant cancer types

The presentation of aberrant peptides at the surface of cancer cells can be exploited for targeted immunotherapy as they imply that cancer cells that developed resistance to therapies targeting their oncogenic mutations still present aberrant peptides following amino acid shortage. To test this possibility, we examined T cell activation in both sensitive and drug-resistant cells. We isolated T cells from OT-1 mice (containing a transgenic T cell receptor that recognizes the SIINFEKL peptide bound to H-2K^b; Hogquist et al., 1994), co-cultured them with A375-H-2K^b and A375-NRAS^{Q61H}-H-2K^b containing either pSloppy$^{C\text{-}SIINFEKL}$ or pSloppy$^{FS\text{-}SIINFEKL}$, that were pre-treated with IFN-γ and the various drug inhibitors (Figures 4A and 4B). The co-cultured cells were maintained in medium containing kynureninase to avoid the production of kynurenine, a well-known inhibitor of T cells, upon tryptophan catabolism by IDO-1 (Figure S4A; Triplett et al., 2018). As expected, the introduction of pSloppy$^{C\text{-}SIINFEKL}$ in A375-H-2K^b provoked T cell recognition, as indicated by the intracellular IFN-γ and tumor necrosis factor α (TNF-α) levels measured by flow cytometry (Figures S4B and S4C). Untreated pSloppy$^{FS\text{-}SIINFEKL}$ cells showed only background levels for both cell lines, consistent with not expressing SIINFEKL peptides (Figures 4C and 4D). Moreover, IFN-γ treatment of both A375 and A375-NRAS^{Q61H} cells expressing pSloppy$^{FS\text{-}SIINFEKL}$ induced T cell activation in an IDO1-dependent manner (Figures 4C and 4D). However, as predicted from our results, only the T cell activation of A375-pSloppy$^{FS\text{-}SIINFEKL}$ was abrogated by vemurafenib, as the addition of vemurafenib to IFN-γ-induced A375-NRAS^{Q61H} cells did not block T cell recognition (Figures 4C and 4D). Finally, we complemented these data using a clonogenic assay (Budhu et al., 2010). A375-pSloppy$^{FS\text{-}SIINFEKL}$ and A375-NRAS^{Q61H}-pSloppy$^{FS\text{-}SIINFEKL}$ were pre-treated for 48 h with IFN-γ, kynureninase, IDOi, or vemurafenib, as indicated. After 48 h, cells were refreshed and exposed for an additional 48 h to OT-1 cells (Figure 4E). *Sloppiness* elicited SIINFEKL-mediated T cell killing that is blocked by IDOi in both cell lines (Figures 4F, 4G, S4D, and S4E). Interestingly, in line with our data, vemurafenib suppressed T cell killing only in the context of A375-pSloppy$^{FS\text{-}SIINFEKL}$ (Figures 4F, 4G, S4D, and S4E).

Figure 4. Aberrant peptide expression elicits T cell recognition and killing

(A) Schematic of how aberrant SIINFEKL peptide presentation induced by IFN-γ-mediated tryptophan depletion leads to T cell tumor recognition. Cells containing pSloppy^{FS}-SIINFEKL are not recognized by T cells in control situations (green T cells), but are predicted to be activated (red T cells) when the tumor cells are exposed to IFN-γ-mediated tryptophan depletion.

(B) Schematic of the experimental procedure. Tumor cells are treated for 24 h with IFN-γ, and then the drugs of interest are added to the medium for an additional 24 h. Subsequently, cells are collected and co-cultured for 12 h with T cells obtained from OT-1 mice before analysis.

(C) A375-H-2K^b-pSloppy^{FS}-SIINFEKL cells were treated for 48 h with IFN-γ, IDOi (300 μM), and the last 24 h with PLX4032 (PLX; 500 nM), as depicted in (B). T cell activation was determined by IFN-γ (upper panel) or TNF (lower panel) levels using flow cytometry. Values represent the average of the 3 independent experiments ± SD. ***$p < 0.001$ by 1-way ANOVA, followed by Bonferroni post hoc test.

(D) Similar to (C), except that A375-NRAS^{Q61H}-H-2K^b-pSloppy^{FS}-SIINFEKL cells were used. Values represent the average of the 3 independent experiments ± SD. **$p < 0.01$, ***$p < 0.001$ by 1-way ANOVA, followed by Bonferroni post hoc test.

(E) A scheme indicating how the stimulation of aberrant protein production can lead to T cell killing of drug-resistant cancer cells.

(F) Bar plots depicting cell viability using a clonogenic assay of A375-H-2K^b-pSloppy^{FS}-SIINFEKL upon T cell attack (Figure S4D). A375-H-2K^b-pSloppy^{FS}-SIINFEKL cells were first treated for 48 h with IFN-γ, with or without IDOi (300 μM), and the last 24 h with vemurafenib (PLX, 500 nM). Afterward, cells were refreshed and co-cultured with OT-1 cells for an additional 24 h. Values represent the average of the 3 independent experiments ± SD. ***$p < 0.001$ by 1-way ANOVA, followed by Sidak post hoc test.

(G) The same assay as in (E), except that A375- NRAS^{Q61H}-H-2K^b-pSloppy^{FS}-SIINFEKL were used. In this assay, 1 μM vemurafenib (PLX) and 200 nM IDOi were used. Values represent the average of the 3 independent experiments ± SD. *$p = 0.04$, **$p = 0.004$, **$p = 0.002$ by 1-way ANOVA, followed by Sidak post hoc test.

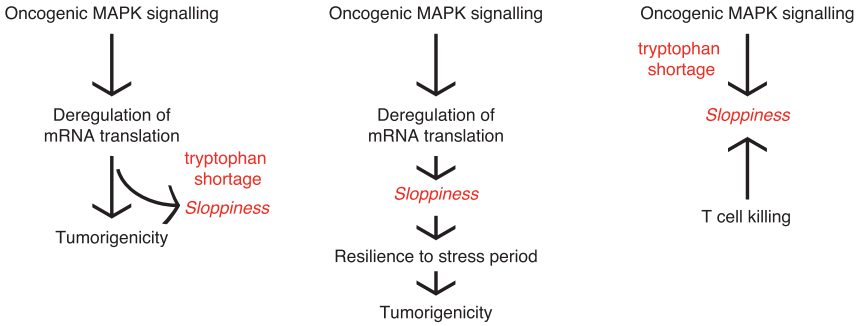

Figure 5. *Sloppiness*, from an adaptive mechanism to a targeting cancer cell opportunity

Left: oncogenic deregulation of the MAPK signaling pathway induces sloppiness when tryptophan is deprived. Middle: the induction of sloppiness in cancer cells can be beneficial to overcome stress period and maintain tumorigenic growth. Right: the induction of sloppiness in cancer cells by tryptophan shortage can be utilized to provoke T cell killing as an anti-tumor immunotherapy strategy.

DISCUSSION

Here, we uncovered *sloppiness*, a widespread mRNA translation phenomenon readily detected in many cancer cell lines, but not in untransformed cells. *Sloppiness* is characterized by the occurrence of ribosomal frameshifting in stress conditions in which the levels of essential amino acids, such as tryptophan, are limiting. The association of *sloppiness* to cancer is reinforced here by the causal link to the oncogenic MAPK pathway. *Sloppiness* was provoked by the expression of oncogenic RAS in primary cell lines and mouse organoids, and was suppressed by inhibitory drugs to various components of the RAS pathway. Moreover, the emergence of acquired resistance to RAS pathway inhibitors fully restored *sloppiness*, indicating specificity. As *sloppiness* leads to the presentation of aberrant peptides and specific induction of T cell killing, its emergence in therapy-resistant conditions suggests therapeutic possibilities. However, the activation of the MAPK pathway seems insufficient, as some non-sloppy cell lines contained oncogenic mutations in KRAS. This indicates a potential role for other factors, such as associated somatic aberrations and cellular contexts, in determining *sloppiness*. Nevertheless, our study strongly links the oncogenic MAPK to *sloppiness* and pinpoints its potential importance in developing novel immunotherapeutic possibilities for therapy-resistant cancers.

RPS6 links hyperactive MAPK pathway to *sloppiness*

We used in this study a reporter vector system to catalog *sloppiness* in human cell lines. This yielded an association to a hyperactive MAPK oncogenic pathway. The link between the MAPK pathway and *sloppiness* appears to be at least in part through RPS6 phosphorylation. The inhibition of RPS6 phosphorylation, either by inhibiting upstream kinases (RPS6AKs) or CRISPR-mediated knockouts of RPS6, suppressed *sloppiness*. The clinical relevance of phosphorylated RPS6 was demonstrated in a pancreatic mouse cancer model, in which it is an important event for tumor initiation (Khalaileh et al., 2013), and in NSCLC, in which it is associated with worse prognosis (Chen et al., 2015). Since some sloppy cell lines have no prominent MAPK mutations, it will be of importance to examine whether they also show high levels of phosphorylated RPS6.

Underlying mechanisms of *sloppiness*

What triggers extensive ribosomal frameshifting in times of amino acid shortage? The simplest possibility is that deregulated mRNA translation in nutrient-deprived conditions results in persistent translation initiation. IFN-γ and tryptophan depletion treatments reduced, but did not fully block, protein synthesis in melanoma cells (Bartok et al., 2021). The sustained loading of ribosomes on mRNAs and their continued elongation during amino acid deprivation is likely to enhance ribosome collisions at the starved codon, which may increase the frequency of sliding and frameshifting. Identifying the underlying mechanisms by which the oncogenic MAPK pathway causes *sloppiness* requires further investigation. As characterized in this study, RPS6 may represent a potential explanation, being a subunit of the 40S ribosome and a player in translation initiation. Identifying the exact mechanisms by which RPS6 phosphorylation and potentially other ribosomal events induce *sloppiness* is of extreme importance to the understanding of its role in tissue development and cancer progression.

Consequences of *sloppiness*

Although *sloppiness* can be simply a by-product of the extensive deregulation of mRNA translation, another attractive possibility is that it may stimulate tumorigenicity by alleviating stress signals originating from colliding ribosomes following amino acid shortage (Figure 5). Recent reports demonstrated that colliding ribosomes induce protein kinases such as ZAKα and GCN2 (EIF2AK4) that enforce proliferation arrest and differentiation by inducing cellular stress pathways (Wu et al., 2020; Vind et al., 2020). Therefore, it is not inconceivable to envision that the deregulation of protein synthesis during cancer development may result in enhanced incidents of colliding ribosomes that would generate stress signals that suppress tumor progression. Cancer-related genetic alterations in the MAPK pathway may stimulate *sloppiness* to moderate cell-cycle arrest and differentiation signals of stressed tumor cells.

T cell therapy

We principally show that aberrant proteins produced by *sloppiness* can be processed and presented at the cell surface, leading to T cell recognition and tumor cell killing (Figure 4). This finding provides the possibility of using immunotherapy to specifically target presented aberrant peptides in otherwise resistant cancers. We foresee that tumor-deprivation procedures can be developed to provoke the synthesis of aberrant proteins in cancers harboring genetic aberrations in the MAPK pathway. These proteins can be processed and presented at the cell surface and

be used for provoking antitumor immunotherapy. In particular, resistant tumors to targeted therapies can benefit from such an approach.

Limitations of the study

In this study, *sloppiness* was described by using reporter vectors that lack regulatory mRNA elements, such as secondary RNA structures, RNA-binding protein sites, and upstream open reading frames, at the 5′ untranslated region (5′ UTR) that can influence translation rate and affect the *sloppiness* of various genes. Nonetheless, IFN-γ treatment of melanoma cells led to the generation of endogenous aberrant peptides that were displayed at the cell surface, reinforcing the conclusions made using our reporters (Bartok et al., 2021). It will be interesting to examine the effect of regulatory elements within 5′ UTRs on *sloppiness*. In addition, the cancer-specific *sloppiness* mechanism described in this article was uncovered based on a limited number of non-transformed cell lines mainly from fibroblast origins. It will be important to expand the description of *sloppiness* and to examine cell types from other tissues, including stem cells and liver cells as they may be more prone to translation errors upon amino acid shortage (Gerashchenko et al., 2020). Addressing these limitations is important for proposing anti-aberrant peptide as an attractive immunotherapy.

STAR★METHODS

Detailed methods are provided in the online version of this paper and include the following:

- KEY RESOURCES TABLE
- RESOURCE AVAILABILITY
  - Lead contact
  - Materials availability
  - Data and code availability
- EXPERIMENTAL MODEL AND SUBJECT DETAILS
  - Mice
  - Crypt isolation and organoid culture
  - Cell culture
  - OT-1 T cells isolation and culture
- METHOD DETAILS
  - Cell treatments
  - Cloning
  - Lentiviral production and transduction
  - Viral transduction of intestinal organoids
  - Amino acid mass spectrometry
  - Analysis of IP-based mass spectrometry data
  - Western blotting
  - qPCR analyses
  - Flow cytometry (SIINFEKL assays)
  - Detection of T cell reactivity
  - T cell killing assay and clonogenic assay
- QUANTIFICATION AND STATISTICAL ANALYSIS

SUPPLEMENTAL INFORMATION

Supplemental information can be found online at https://doi.org/10.1016/j.molcel.2021.09.002.

ACKNOWLEDGMENTS

R.A. is supported by the Dutch Cancer Society (KWF projects 13647, 11574), the European Research Council (ERC-PoC #665317 and ERC-AdG #832844), and the Dutch Science Organization (NWO-TOP #91216002). A.P. is supported by a long-term EMBO fellowship grant (EMBO ALTF 796-2018). O.B.B. and M.A. are supported by the Dutch NWO X-omics Initiative. We are grateful to George Georgiou and Everett Stone for the kynureninase gift. We would like to express our thanks to all of the members of the Agami lab for very fruitful discussions.

AUTHOR CONTRIBUTIONS

R.A. conceived and supervised the project and wrote the manuscript. J.C. conceived the project, designed and performed the experiments, analyzed the data, and wrote the manuscript. A.P, conceived the project, performed the bioinformatics analysis, and wrote the manuscript. N.B., R.N., D.W., and S.R. conducted some of the biological experiments. O.B.B. and M.A. performed the mass spectrometry analysis. E.A.Z. and C.R.B. performed the amino acid metabolomics analyses. J.K., D.S.P., and W.J.F. provided the reagents, technical assistance, and feedback.

DECLARATION OF INTERESTS

The authors declare no competing interests.

Received: February 22, 2021
Revised: July 13, 2021
Accepted: August 30, 2021
Published: September 24, 2021

REFERENCES

Akar, U., Ozpolat, B., Mehta, K., Lopez-Berestein, G., Zhang, D., Ueno, N.T., Hortobagyi, G.N., and Arun, B. (2010). Targeting p70S6K prevented lung metastasis in a breast cancer xenograft model. Mol. Cancer Ther. *9*, 1180–1187.

Aoki, M., Blazek, E., and Vogt, P.K. (2001). A role of the kinase mTOR in cellular transformation induced by the oncoproteins P3k and Akt. Proc. Natl. Acad. Sci. USA *98*, 136–141.

Baranov, P.V., Wills, N.M., Barriscale, K.A., Firth, A.E., Jud, M.C., Letsou, A., Manning, G., and Atkins, J.F. (2011). Programmed ribosomal frameshifting in the expression of the regulator of intestinal stem cell proliferation, adenomatous polyposis coli (APC). RNA Biol. *8*, 637–647.

Barna, M., Pusic, A., Zollo, O., Costa, M., Kondrashov, N., Rego, E., Rao, P.H., and Ruggero, D. (2008). Suppression of Myc oncogenic activity by ribosomal protein haploinsufficiency. Nature *456*, 971–975.

Bartok, O., Pataskar, A., Nagel, R., Laos, M., Goldfarb, E., Hayoun, D., Levy, R., Korner, P.R., Kreuger, I.Z.M., Champagne, J., et al. (2021). Anti-tumour immunity induces aberrant peptide presentation in melanoma. Nature *590*, 332–337.

Bhat, M., Robichaud, N., Hulea, L., Sonenberg, N., Pelletier, J., and Topisirovic, I. (2015). Targeting the translation machinery in cancer. Nat. Rev. Drug Discov. *14*, 261–278.

Brandman, O., and Hegde, R.S. (2016). Ribosome-associated protein quality control. Nat. Struct. Mol. Biol. *23*, 7–15.

Budhu, S., Loike, J.D., Pandolfi, A., Han, S., Catalano, G., Constantinescu, A., Clynes, R., and Silverstein, S.C. (2010). CD8+ T cell concentration determines their efficiency in killing cognate antigen-expressing syngeneic mammalian cells in vitro and in mouse tissues. J. Exp. Med. *207*, 223–235.

Chen, B., Tan, Z., Gao, J., Wu, W., Liu, L., Jin, W., Cao, Y., Zhao, S., Zhang, W., Qiu, Z., et al. (2015). Hyperphosphorylation of ribosomal protein S6 predicts unfavorable clinical survival in non-small cell lung cancer. J. Exp. Clin. Cancer Res. *34*, 126.

Clark, M.B., Jänicke, M., Gottesbühren, U., Kleffmann, T., Legge, M., Poole, E.S., and Tate, W.P. (2007). Mammalian gene PEG10 expresses two reading frames by high efficiency -1 frameshifting in embryonic-associated tissues. J. Biol. Chem. *282*, 37359–37369.

Dersh, D., Yewdell, J.W., and Wei, J. (2019). A SIINFEKL-Based System to Measure MHC Class I Antigen Presentation Efficiency and Kinetics. Methods Mol. Biol. *1988*, 109–122.

Dever, T.E., Dinman, J.D., and Green, R. (2018). Translation Elongation and Recoding in Eukaryotes. Cold Spring Harb. Perspect. Biol. *10*, a032649.

Di Nicolantonio, F., Arena, S., Tabernero, J., Grosso, S., Molinari, F., Macarulla, T., Russo, M., Cancelliere, C., Zecchin, D., Mazzucchelli, L., et al. (2010). Deregulation of the PI3K and KRAS signaling pathways in human cancer cells determines their response to everolimus. J. Clin. Invest. *120*, 2858–2866.

Dinman, J.D. (2012). Mechanisms and implications of programmed translational frameshifting. Wiley Interdiscip. Rev. RNA *3*, 661–673.

Ebright, R.Y., Lee, S., Wittner, B.S., Niederhoffer, K.L., Nicholson, B.T., Bardia, A., Truesdell, S., Wiley, D.F., Wesley, B., Li, S., et al. (2020). Deregulation of ribosomal protein expression and translation promotes breast cancer metastasis. Science *367*, 1468–1473.

Fang, Y., Treffers, E.E., Li, Y., Tas, A., Sun, Z., van der Meer, Y., de Ru, A.H., van Veelen, P.A., Atkins, J.F., Snijder, E.J., and Firth, A.E. (2012). Efficient -2 frameshifting by mammalian ribosomes to synthesize an additional arterivirus protein. Proc. Natl. Acad. Sci. USA *109*, E2920–E2928.

Farabaugh, P.J. (1996). Programmed translational frameshifting. Microbiol. Rev. *60*, 103–134.

Fingar, D.C., and Blenis, J. (2004). Target of rapamycin (TOR): an integrator of nutrient and growth factor signals and coordinator of cell growth and cell cycle progression. Oncogene *23*, 3151–3171.

Gerashchenko, M.V., Nesterchuk, M.V., Smekalova, E.M., Paulo, J.A., Kowalski, P.S., Akulich, K.A., Bogorad, R., Dmitriev, S.E., Gygi, S., Zatsepin, T., et al. (2020). Translation elongation factor 2 depletion by siRNA in mouse liver leads to mTOR-independent translational upregulation of ribosomal protein genes. Sci. Rep. *10*, 15473.

Goldberg, A.L., Cascio, P., Saric, T., and Rock, K.L. (2002). The importance of the proteasome and subsequent proteolytic steps in the generation of antigenic peptides. Mol. Immunol. *39*, 147–164.

Hogquist, K.A., Jameson, S.C., Heath, W.R., Howard, J.L., Bevan, M.J., and Carbone, F.R. (1994). T cell receptor antagonist peptides induce positive selection. Cell *76*, 17–27.

Hsieh, A.C., Costa, M., Zollo, O., Davis, C., Feldman, M.E., Testa, J.R., Meyuhas, O., Shokat, K.M., and Ruggero, D. (2010). Genetic dissection of the oncogenic mTOR pathway reveals druggable addiction to translational control via 4EBP-eIF4E. Cancer Cell *17*, 249–261.

Hsieh, A.C., Liu, Y., Edlind, M.P., Ingolia, N.T., Janes, M.R., Sher, A., Shi, E.Y., Stumpf, C.R., Christensen, C., Bonham, M.J., et al. (2012). The translational landscape of mTOR signalling steers cancer initiation and metastasis. Nature *485*, 55–61.

Hua, H., Kong, Q., Zhang, H., Wang, J., Luo, T., and Jiang, Y. (2019). Targeting mTOR for cancer therapy. J. Hematol. Oncol. *12*, 71.

Hugo, W., Shi, H., Sun, L., Piva, M., Song, C., Kong, X., Moriceau, G., Hong, A., Dahlman, K.B., Johnson, D.B., et al. (2015). Non-genomic and Immune Evolution of Melanoma Acquiring MAPKi Resistance. Cell *162*, 1271–1285.

Ishimura, R., Nagy, G., Dotu, I., Chuang, J.H., and Ackerman, S.L. (2016). Activation of GCN2 kinase by ribosome stalling links translation elongation with translation initiation. eLife *5*, e14295.

Ivanov, I.P., and Atkins, J.F. (2007). Ribosomal frameshifting in decoding antizyme mRNAs from yeast and protists to humans: close to 300 cases reveal remarkable diversity despite underlying conservation. Nucleic Acids Res. *35*, 1842–1858.

Jackson, R.J., Hellen, C.U., and Pestova, T.V. (2010). The mechanism of eukaryotic translation initiation and principles of its regulation. Nat. Rev. Mol. Cell Biol. *11*, 113–127.

Jefferies, H.B., Fumagalli, S., Dennis, P.B., Reinhard, C., Pearson, R.B., and Thomas, G. (1997). Rapamycin suppresses 5′TOP mRNA translation through inhibition of p70s6k. EMBO J. *16*, 3693–3704.

Ketteler, R. (2012). On programmed ribosomal frameshifting: the alternative proteomes. Front. Genet. *3*, 242.

Khalaileh, A., Dreazen, A., Khatib, A., Apel, R., Swisa, A., Kidess-Bassir, N., Maitra, A., Meyuhas, O., Dor, Y., and Zamir, G. (2013). Phosphorylation of ribosomal protein S6 attenuates DNA damage and tumor suppression during development of pancreatic cancer. Cancer Res. *73*, 1811–1820.

Kosnopfel, C., Sinnberg, T., Sauer, B., Niessner, H., Schmitt, A., Makino, E., Forschner, A., Hailfinger, S., Garbe, C., and Schittek, B. (2017). Human melanoma cells resistant to MAPK inhibitors can be effectively targeted by inhibition of the p90 ribosomal S6 kinase. Oncotarget *8*, 35761–35775.

Krieg, J., Hofsteenge, J., and Thomas, G. (1988). Identification of the 40 S ribosomal protein S6 phosphorylation sites induced by cycloheximide. J. Biol. Chem. *263*, 11473–11477.

Lin, L., Sabnis, A.J., Chan, E., Olivas, V., Cade, L., Pazarentzos, E., Asthana, S., Neel, D., Yan, J.J., Lu, X., et al. (2015). The Hippo effector YAP promotes resistance to RAF- and MEK-targeted cancer therapies. Nat. Genet. *47*, 250–256.

Liu, G.Y., and Sabatini, D.M. (2020). mTOR at the nexus of nutrition, growth, ageing and disease. Nat. Rev. Mol. Cell Biol. *21*, 183–203.

Ma, X.M., and Blenis, J. (2009). Molecular mechanisms of mTOR-mediated translational control. Nat. Rev. Mol. Cell Biol. *10*, 307–318.

Malka-Mahieu, H., Newman, M., Désaubry, L., Robert, C., and Vagner, S. (2017). Molecular Pathways: The eIF4F Translation Initiation Complex-New Opportunities for Cancer Treatment. Clin. Cancer Res. *23*, 21–25.

Maru, Y., Orihashi, K., and Hippo, Y. (2016). Lentivirus-Based Stable Gene Delivery into Intestinal Organoids. Methods Mol. Biol. *1422*, 13–21.

McCarthy, M.K., and Weinberg, J.B. (2015). The immunoproteasome and viral infection: a complex regulator of inflammation. Front. Microbiol. *6*, 21.

Meydan, S., Klepacki, D., Karthikeyan, S., Margus, T., Thomas, P., Jones, J.E., Khan, Y., Briggs, J., Dinman, J.D., Vázquez-Laslop, N., and Mankin, A.S. (2017). Programmed Ribosomal Frameshifting Generates a Copper Transporter and a Copper Chaperone from the Same Gene. Mol. Cell *65*, 207–219.

Moyano-Galceran, L., Pietilä, E.A., Turunen, S.P., Corvigno, S., Hjerpe, E., Bulanova, D., Joneborg, U., Alkasalias, T., Miki, Y., Yashiro, M., et al. (2020). Adaptive RSK-EphA2-GPRC5A signaling switch triggers chemotherapy resistance in ovarian cancer. EMBO Mol. Med. *12*, e11177.

Okamura, K., Feuk, L., Marquès-Bonet, T., Navarro, A., and Scherer, S.W. (2006). Frequent appearance of novel protein-coding sequences by frameshift translation. Genomics *88*, 690–697.

Pelletier, J., Graff, J., Ruggero, D., and Sonenberg, N. (2015). Targeting the eIF4F translation initiation complex: a critical nexus for cancer development. Cancer Res. *75*, 250–263.

Penn, W.D., Harrington, H.R., Schlebach, J.P., and Mukhopadhyay, S. (2020). Regulators of Viral Frameshifting: More Than RNA Influences Translation Events. Annu. Rev. Virol. *7*, 219–238.

Perez-Riverol, Y., Csordas, A., Bai, J., Bernal-Llinares, M., Hewapathirana, S., Kundu, D.J., Inuganti, A., Griss, J., Mayer, G., Eisenacher, M., et al. (2019). The PRIDE database and related tools and resources in 2019: improving support for quantification data. Nucleic Acids Res. *47* (D1), D442–D450.

Pyronnet, S., Imataka, H., Gingras, A.C., Fukunaga, R., Hunter, T., and Sonenberg, N. (1999). Human eukaryotic translation initiation factor 4G (eIF4G) recruits mnk1 to phosphorylate eIF4E. EMBO J. *18*, 270–279.

Rapino, F., Delaunay, S., Rambow, F., Zhou, Z., Tharun, L., De Tullio, P., Sin, O., Shostak, K., Schmitz, S., Piepers, J., et al. (2018). Codon-specific translation reprogramming promotes resistance to targeted therapy. Nature *558*, 605–609.

Roux, P.P., Shahbazian, D., Vu, H., Holz, M.K., Cohen, M.S., Taunton, J., Sonenberg, N., and Blenis, J. (2007). RAS/ERK signaling promotes

site-specific ribosomal protein S6 phosphorylation via RSK and stimulates cap-dependent translation. J. Biol. Chem. *282*, 14056–14064.

Ruggero, D., Montanaro, L., Ma, L., Xu, W., Londei, P., Cordon-Cardo, C., and Pandolfi, P.P. (2004). The translation factor eIF-4E promotes tumor formation and cooperates with c-Myc in lymphomagenesis. Nat. Med. *10*, 484–486.

Sato, T., Vries, R.G., Snippert, H.J., van de Wetering, M., Barker, N., Stange, D.E., van Es, J.H., Abo, A., Kujala, P., Peters, P.J., and Clevers, H. (2009). Single Lgr5 stem cells build crypt-villus structures in vitro without a mesenchymal niche. Nature *459*, 262–265.

Shigemoto, K., Brennan, J., Walls, E., Watson, C.J., Stott, D., Rigby, P.W., and Reith, A.D. (2001). Identification and characterisation of a developmentally regulated mammalian gene that utilises -1 programmed ribosomal frameshifting. Nucleic Acids Res. *29*, 4079–4088.

Siu, F., Bain, P.J., LeBlanc-Chaffin, R., Chen, H., and Kilberg, M.S. (2002). ATF4 is a mediator of the nutrient-sensing response pathway that activates the human asparagine synthetase gene. J. Biol. Chem. *277*, 24120–24127.

Smith, A.M., Costello, M.S., Kettring, A.H., Wingo, R.J., and Moore, S.D. (2019). Ribosome collisions alter frameshifting at translational reprogramming motifs in bacterial mRNAs. Proc. Natl. Acad. Sci. USA *116*, 21769–21779.

Triplett, T.A., Garrison, K.C., Marshall, N., Donkor, M., Blazeck, J., Lamb, C., Qerqez, A., Dekker, J.D., Tanno, Y., Lu, W.C., et al. (2018). Reversal of indoleamine 2,3-dioxygenase-mediated cancer immune suppression by systemic kynurenine depletion with a therapeutic enzyme. Nat. Biotechnol. *36*, 758–764.

Truitt, M.L., and Ruggero, D. (2017). New frontiers in translational control of the cancer genome. Nat. Rev. Cancer *17*, 332.

Truitt, M.L., Conn, C.S., Shi, Z., Pang, X., Tokuyasu, T., Coady, A.M., Seo, Y., Barna, M., and Ruggero, D. (2015). Differential Requirements for eIF4E Dose in Normal Development and Cancer. Cell *162*, 59–71.

Tuller, T., Carmi, A., Vestsigian, K., Navon, S., Dorfan, Y., Zaborske, J., Pan, T., Dahan, O., Furman, I., and Pilpel, Y. (2010). An evolutionarily conserved mechanism for controlling the efficiency of protein translation. Cell *141*, 344–354.

Tyanova, S., Temu, T., and Cox, J. (2016). The MaxQuant computational platform for mass spectrometry-based shotgun proteomics. Nat. Protoc. *11*, 2301–2319.

van Es, J.H., and Clevers, H. (2015). Generation and analysis of mouse intestinal tumors and organoids harboring APC and K-Ras mutations. Methods Mol. Biol. *1267*, 125–144.

Vind, A.C., Genzor, A.V., and Bekker-Jensen, S. (2020). Ribosomal stress-surveillance: three pathways is a magic number. Nucleic Acids Res. *48*, 10648–10661.

Voorhoeve, P.M., and Agami, R. (2003). The tumor-suppressive functions of the human INK4A locus. Cancer Cell *4*, 311–319, 14585358.

Voorhoeve, P.M., le Sage, C., Schrier, M., Gillis, A.J., Stoop, H., Nagel, R., Liu, Y.P., van Duijse, J., Drost, J., Griekspoor, A., et al. (2006). A genetic screen implicates miRNA-372 and miRNA-373 as oncogenes in testicular germ cell tumors. Cell *124*, 1169–1181.

Wagle, N., Van Allen, E.M., Treacy, D.J., Frederick, D.T., Cooper, Z.A., Taylor-Weiner, A., Rosenberg, M., Goetz, E.M., Sullivan, R.J., Farlow, D.N., et al. (2014). MAP kinase pathway alterations in BRAF-mutant melanoma patients with acquired resistance to combined RAF/MEK inhibition. Cancer Discov. *4*, 61–68.

Wang, L., Leite de Oliveira, R., Huijberts, S., Bosdriesz, E., Pencheva, N., Brunen, D., Bosma, A., Song, J.Y., Zevenhoven, J., Los-de Vries, G.T., et al. (2018). An Acquired Vulnerability of Drug-Resistant Melanoma with Therapeutic Potential. Cell *173*, 1413–1425.e14.

Wang, X., Xuan, Y., Han, Y., Ding, X., Ye, K., Yang, F., Gao, P., Goff, S.P., and Gao, G. (2019). Regulation of HIV-1 Gag-Pol Expression by Shiftless, an Inhibitor of Programmed -1 Ribosomal Frameshifting. Cell *176*, 625–635.e14.

Waskiewicz, A.J., Johnson, J.C., Penn, B., Mahalingam, M., Kimball, S.R., and Cooper, J.A. (1999). Phosphorylation of the cap-binding protein eukaryotic translation initiation factor 4E by protein kinase Mnk1 in vivo. Mol. Cell. Biol. *19*, 1871–1880.

Weiss, R., and Gallant, J. (1983). Mechanism of ribosome frameshifting during translation of the genetic code. Nature *302*, 389–393.

Wu, C.C., Peterson, A., Zinshteyn, B., Regot, S., and Green, R. (2020). Ribosome Collisions Trigger General Stress Responses to Regulate Cell Fate. Cell *182*, 404–416.e14.

Yan, S., Wen, J.D., Bustamante, C., and Tinoco, I., Jr. (2015). Ribosome excursions during mRNA translocation mediate broad branching of frameshift pathways. Cell *160*, 870–881.

Ye, J., Kumanova, M., Hart, L.S., Sloane, K., Zhang, H., De Panis, D.N., Bobrovnikova-Marjon, E., Diehl, J.A., Ron, D., and Koumenis, C. (2010). The GCN2-ATF4 pathway is critical for tumour cell survival and proliferation in response to nutrient deprivation. EMBO J. *29*, 2082–2096.

STAR★METHODS

KEY RESOURCES TABLE

REAGENT or RESOURCE	SOURCE	IDENTIFIER
Antibodies		
Mouse anti-human HSP60	Cell Signaling	Catalog # 4869; RRID: AB_2264430
Mouse anti-human HSP90	BD Biosciences	Catalog # 610418; RRID: AB_397798
Mouse anti-human p44/42 MAPK (Erk1/2) (L34F12)	Cell Signaling	Catalog # 4696; RRID: AB_390780
Mouse anti-human p53 (DO-1)	Santa Cruz Biotechnology	Catalog # 2215; RRID: AB_331682
Mouse anti-human S6 Ribosomal Protein (54D2)	Cell Signaling	Catalog # 2317; RRID: AB_2238583
Mouse anti-V5 tag	Thermo Fisher Scientific	Catalog # R960-25; RRID: AB_2556564
Rabbit anti-human IDO (D5J4E)	Cell Signaling	Catalog # 86630; RRID: AB_2636818
Rabbit anti-human p-21 (C-19)	Santa Cruz Biotechnology	Catalog # sc-397; RRID: AB_632126
Rabbit anti-human Phospho-p44/42 MAPK (Erk1/2) (Thr202/Tyr204)	Cell Signaling	Catalog # 9101; RRID: AB_331646
Rabbit anti-human Phospho-S6 Ribosomal Protein (Ser235/236)	Cell Signaling	Catalog #2211; RRID: AB_331679
Rabbit anti-human Phospho-S6 Ribosomal Protein (Ser240/244)	Cell Signaling	Catalog # 2215; RRID: AB_331682
Rabbit anti-turboGFP tag	Thermo Fisher Scientific	Catalog # PA5-22688; RRID: AB_2540616
Rabbit anti-turboGFP tag	Evrogen	Catalog # AB513
Rat anti-human alpha-Tubulin (YL1)	Santa Cruz Biotechnology	Catalog # sc-53029; RRID: AB_793541
Rat anti-human H-Ras	Santa Cruz Biotechnology	Catalog # sc-35; RRID: AB_627749
IRDye® 680RD donkey anti-mouse Secondary Antibody	Li-COR	Catalog # 926-68072; RRID: AB_10953628
IRDye® 680RD donkey anti-rabbit Secondary Antibody	Li-COR	Catalog #926-68073 ; RRID: AB_10954442
IRDye® 800CW goat anti-mouse Secondary Antibody	Li-COR	Catalog #926-32350 ; RRID: AB_2782997
IRDye® 800CW goat anti-rabbit Secondary Antibody	Li-COR	Catalog # 926-32211; RRID: AB_621843
IRDye® 800CW Goat anti-Rat IgG Secondary Antibody	Li-COR	Catalog # 926-32219; RRID: AB_1850025
APC anti-mouse H-2Kb bound to SIINFEKL clone 25-D1.16	Biolegend	Catalog # 141606; RRID: AB_11219595
APC anti-mouse IFNgamma	Miltenyi	Catalog # 130-120-805; RRID: AB_2784369
PE anti-mouse TNFalpha	Miltenyi	Catalog # 130-102-386; RRID: AB_2661141
vioblue anti-mouse CD8b	Miltenyi	Catalog # 130-106-312; RRID: AB_2659560
Bacterial and virus strains		
DH5-alpha	Thermo Fisher Scientific	Catalog# 18265017
Chemicals, peptides, and recombinant proteins		
(Z)-4-Hydroxytamoxifen	Sigma Aldrich	Catalog # H7904
1-Methyl-L-tryptophan (IDO1 inhibitor)	Sigma Aldrich	Catalog # 447439
10X-Tris Glycine	Thermo Fisher Scientific	Catalog # BP1306-4
10X-Tris Glycine-SDS	Bio-rad	Catalog # 1610772
2-Mercaptoethanol	Sigma Aldrich	Catalog # M6250
2-Propanol	Sigma Aldrich	Catalog # I9516
Acetic Acid	Sigma Aldrich	Catalog # A6283
Acrylamide/Bis solution, 37.5:1	Bio-rad	Catalog # 1610149
Advanced DMEM/F12	Thermo Fisher Scientific	Catalog # 12634-010
Animal-Free Recombinant Murine EGF	Peprotech	Catalog # AF-315-09
B-27 Supplement (50X), minus vitamin A	Thermo Fisher Scientific	Catalog # 12587010
BamH1-HF	New England BioLabs	Catalog # R0136
BCA Protein Assay Kit	Thermo Fisher Scientific	Catalog # 23225
BD GolgiPlug Protein Transport Inhibitor	BD Biosciences	Catalog # 555029
Blasticidin S Hydrochloride	Thermo Fisher Scientific	Catalog # 10264913
Bovine Serum Albumin	Sigma Aldrich	Catalog # A9647

(*Continued on next page*)

Continued

REAGENT or RESOURCE	SOURCE	IDENTIFIER
Bovine Serum Albumin	Sigma Aldrich	Catalog # A9647
BsmBI	New England BioLabs	Catalog # R0734L
CHIR99021	Cayman chemical	Catalog # 13122-5
Chloroform	Sigma Aldrich	Catalog # 288306
Crystal violet solution	Sigma Aldrich	Catalog # V5265
Cultrex Reduced Growth Factor Basement Membrane Extract	R&D Systems	Catalog # 3533-010-02
DAPI (4',6-Diamidino-2-Phenylindole, Dihydrochloride)	Thermo Fisher Scientific	Catalog # D1306
DMEM without tyrosine	Cell Culture Technologies	Custom-made
DMEM/F-12, HEPES	Thermo Fisher Scientific	Catalog # 31330095
DMSO	Sigma Aldrich	Catalog # 34943
Doxorubicin	Selleckchem	Catalog # S1208
Dulbecco's MEM (DMEM) F-12 w/o Tryptophan	USBiological life Sciences	Catalog # D9807-04-10
Dynabeads Protein G for Immunoprecipitation	Thermo Fisher Scientific	Catalog # 10004D
eBioscience Foxp3 / Transcription Factor Staining Buffer Set	Thermo Fisher Scientific	Catalog # 00-5523-00
EcoRI	New England BioLabs	Catalog # R3101L
EGF, human recombinant	Millipore	Catalog # 01-107
Epacadostat	Medkoo	Catalog # 206461
Ethidium Bromide Solution	Bio-connect	Catalog # 04802511
FastAP	Thermo Fisher Scientific	Catalog # EF0654
Fetal Bovine Serum (discontinued)	Sigma Aldrich	Catalog # 31011120
Fetal Bovine Serum, dialyzed US origin	Thermo Fisher Scientific	Catalog # 26400044
Formaldehyde solution	Sigma Aldrich	Catalog # 252549
Gefitinib (ZD1839)	Sellekchem	Catalog # S1025
GIBCO DMEM, high glucose, pyruvate	Thermo Fisher Scientific	Catalog # 41966052
GIBCO HEPES (1M)	Thermo Fisher Scientific	Catalog # 15630056 or # 15630-080
GlutaMAX Supplement	Thermo Fisher Scientific	Catalog # 35050038
Hexadimethrine bromide	Sigma Aldrich	Catalog # H9268
Horse Serum	Thermo Fisher Scientific	Catalog # 16050130
Human recombinant interferon gamma	Peprotech	Catalog # 300-02
Hydrocortisone	Sigma Aldrich	Catalog # H0888
Hygromycin B	Thermo Fisher Scientific	Catalog # 10687010
Il-15	ImmunoTools	N/A
IL-2	Proleukin, Novartis	N/A
IL-7	Immunotools	N/A
Insulin from bovine pancreas	Sigma Aldrich	Catalog # I1882
Ionomycin	Sigma Aldrich	Catalog # I9657
Jagged - 1 (188 - 204), Notch Ligand, DSL Peptide	Anaspec	Catalog # AS-61298
Kynureninase (Kynase)	Kind Gift	N/A
L-Glutamine 200 mM (100x)	Thermo Fisher Scientific	Catalog # 25030123
L-tryptophan	Sigma Aldrich	Catalog # T0254
Lenti-X Concentrator	Takara	Catalog # 631232
Live/dead fixable near-IR dead cell stain kit	Thermo Fisher Scientific	Catalog # L10119
MG-132 proteasome inhibitor	Selleckchem	Catalog # S2619
N-2 Supplement (100X)	Thermo Fisher Scientific	Catalog # 17502048
Nitrocellulose membrane 0.22 uM pore size	Santa Cruz	Catalog # sc-3718
Nocodazole	Selleckchem	Catalog # S2775
NotI-HF	New England BioLabs	Catalog # R3189L
PBS tablets	Thermo Fisher Scientific	Catalog # 18912014
PD-0332991	Kind Gift from W.Faller	N/A

(*Continued on next page*)

Continued

REAGENT or RESOURCE	SOURCE	IDENTIFIER
Penicillin/streptomycin	Thermo Fisher Scientific	Catalog # 15140148
Phorbol 12-myristate 13-acetate (PMA)	Sigma Aldrich	Catalog # 19-144
Phusion HF DNA Polymerase	Thermo Fisher Scientific	Catalog # F530
Polyethylenimine Hydrochloride	Polysciences	Catalog # 25439-2
Pooled Human Serum	One Lamdba	Catalog # A25761
Puromycin	Bio-connect	Catalog # AG-CN2-0078-M500
pyridoxal 5′-phosphate hydrate	Sigma Aldrich	Catalog # P9255
Pyridoxal 5′-phosphate hydrate (PLP)	Sigma-Aldrich	Catalog # P3657
Recombinant Murine Noggin	Peprotech	Catalog # 00-5523-00
Recombinant murine R-spondin-1	Peprotech	Catalog # 315-32
Rho kinase inhibitor Y-27632	Cayman chemical	Catalog # 10005583
RPMI 1640 Medium	Thermo Fisher Scientific	Catalog # 21875-091
Sodium bicarbonate	Sigma Aldrich	Catalog # S6014
StemPro Accutase Cell Dissociation Reagent	Thermo Fisher Scientific	Catalog # A1110501
T4 DNA Ligase	New England BioLabs	Catalog # M0202
T4 PNK	New England BioLabs	Catalog # M0201L
Torin-1	Tocris Bioscience	Catalog # 4247
Trametinib (GSK1120212)	Sellekchem	Catalog # S2673
Trizol	Thermo Fisher Scientific	Catalog # 15596018
Tween 20	Sigma Aldrich	Catalog # P1379
Ultra-pure 0,5M EDTA pH8.0	Thermo Fisher Scientific	Catalog # 15575-038
Ultrapure DNase/RNase free water	Thermo Fisher Scientific	Catalog # 10977015
Valproic Acid, Sodium Salt	BioVision	Catalog # 1647-200
Vemurafenib (PLX4032, RG7204)	MedKoo	Catalog # 202271
Versene solution-100 ml	Thermo Fisher Scientific	Catalog # 15040033
XbaI	Thermo Fisher Scientific	Catalog # ER0682
Critical commercial assays		
Dynabeads Untouched Mouse CD8 Cells Kit	Thermo Fisher Scientific	Catalog # 11417D
EZ-PCR Mycoplasma Detection Kit	Biological Industries	Catalog # 20-700-20
LJH685-5mg	Selleckchem	Catalog # S7870
QIAquick PCR Purification Kit	QIAGEN	Catalog # 28106
PureLink® Quick Maxiprep Kit	Thermo Fisher Scientific	Catalog # K210007
PureLink® Quick Midiprep Kit	Thermo Fisher Scientific	Catalog # K210004
PureLink® Quick Miniprep Kit	Thermo Fisher Scientific	Catalog # K210002
SensiFAST SYBR® No-ROX Kit	Bioline	Catalog # BIO-98050
Tetro reverse Transcriptase	Bioline	Catalog # BIO-65050
Wizard SV Gel and PCR Clean-Up System	Promega	Catalog # A9282
Deposited data		
Mass-spec	Pride	PXD022707
Experimental models: cell lines		
108T	Bartok et al., 2021	N/A
293T	Internal stock	RRID:CVCL_0063
A-375	Bartok et al. (2021)	RRID:CVCL_0132
A-375DR	Wang et al. (2018)	N/A
A549	Internal stock	RRID:CVCL_0023
Aspc-1	Internal stock	RRID:CVCL_0152
BJ-EHT	Voorhoeve and Agami, 2003	N/A
BJ-EHT p53KD iHRASG12V	Voorhoeve et al. (2006)	N/A

(*Continued on next page*)

Continued

REAGENT or RESOURCE	SOURCE	IDENTIFIER
BT-474	Internal stock	RRID:CVCL_0179
BT-549	Internal stock	RRID:CVCL_1092
Capan-1	Internal stock	RRID:CVCL_0237
D10	Gift from D. Peeper	RRID:CVCL_H945
HCC827	Internal stock	RRID:CVCL_2063
HCT 116	Internal stock	RRID:CVCL_0291
HT-29	Internal stock	RRID:CVCL_0320
hTERT RPE-1	Internal stock	RRID:CVCL_4388
LS174T	Internal stock	RRID:CVCL_0397
MCF 10A	Internal stock	RRID:CVCL_0598
MCF-7	Internal stock	RRID:CVCL_0031
MD55A-3	Bartok et al. (2021)	N/A
MDA-MB-231	Internal stock	RRID:CVCL_0062
MDA-MB-468	Internal stock	RRID:CVCL_0419
MIA Paca-2	Internal stock	RRID:CVCL_0428
NCI-H1299	Internal stock	RRID:CVCL_0060
NCI-H358	Internal stock	RRID:CVCL_1559
OVCAR-3	Internal stock	RRID:CVCL_0465
OVCAR-4	Internal stock	RRID:CVCL_1627
PC-3	Internal stock	RRID:CVCL_0035
SK-MEL-28	Internal stock	RRID:CVCL_0526
SK-OV-3	Internal stock	RRID:CVCL_0532
SW1573	Internal stock	RRID:CVCL_1720
SW480	Internal stock	RRID:CVCL_1724
T-47D	Internal stock	RRID:CVCL_0553
TIG-3	Gift from D. Peeper	N/A
U-2 OS	Internal stock	RRID:CVCL_0042
U-87 MG	Internal stock	RRID:CVCL_0022
WiDR	Internal stock	RRID:CVCL_2760
ZR-75-1	Internal stock	RRID:CVCL_0588
Experimental models: organisms/strains		
C57BL/6J VillinCre^{Ert2} and VillinCre^{Ert2} APC$^{fl/fl}$ KRAS$^{G12D/+}$ (no gender specificity)	van Es and Clevers (2015)	N/A
Oligonucleotides		
ACAGCGTCTAGAGCCACCATGGGTAAGCCTATCCCTAACCCT CTCCTCGGTCTCGATTCTACGGGCGGCGGTAAGCCTATCCCT AACCCTCTCCTCGGTCTCGATTCTACGGGCGGCACCGAAATG AGCTTCCTGAG	This paper	V5-ATF4-For
CCGAATGGCTCGCTGTCGGAGGAATGGAGAGCGACG	This paper	ATF4-tGFP for
CCGAATGGCTCGCTGTCGGAGGATATGGAGAGCGACG	This paper	ATF4+1-tGFP for
ACAGCGGCGGCCGCTCAGTTATCTATTCTTCACCGGCATC	This paper	tGFP rev
ACAGCGGCGGCCGCTCAGCTATTTAGAGCTTTTCGAAGTTG ATGATGGATTCCAGCT GCTCGAGTTCTTCACCGGCATCTGC	This paper	tGFP-SIINFEKL rev
TATATTCTAGAGCCACCATGGACTACAaAGACGATGACGATAAAG	This paper	Flag-YAP For
TATAGAATTCTCAGCTATTTAtaaccatgtaagaaagctttctttatctagcttg	This paper	YAP Rev
TATATTCTAGAGCCACCATGGTACCGTGCACGCTG	This paper	H2Kb For
ACAGCGGAATTCTCACGCTAGAGAATGAGG	This paper	H2Kb Rev
ACAGCGGGATCCCGCCTTTTCCAAGGCAGCC	This paper	Hygro For

(*Continued on next page*)

Continued

REAGENT or RESOURCE	SOURCE	IDENTIFIER
ACAGCGCTCGAGTCATTCCTTGGCTCTGGGTC	This paper	Hygro Rev
GCTGAGGATTTGGAAAGGGT	This paper	HPRT1-For#1 qPCR
CATCTCGAGCAAGACGTTCA	This paper	HPRT1-Rev#1 qPCR
TGACACTGGCAAAACAATGCA	This paper	HPRT1-For#2 qPCR
GGTCCTTTTCACCAGCAAGCT	This paper	HPRT1-Rev#2 qPCR
GCGCAGATCGAACTACTGCT	This paper	ASNS-For#1 qPCR
CATTTCTGGTGGCAGAGACAA	This paper	ASNS-Rev#1 qPCR
CACATCACCCTGACCTGCTT	This paper	ASNS-For#2 qPCR
CTCACCATCCACTTTGGTCTG	This paper	ASNS-Rev#2 qPCR
CACCGAGTGGTGGGAACGACAAACA	This paper	For-RPS6-sgRNA
AAACTGTTTGTCGTTCCCACCACTC	This paper	Rev-RPS6-sgRNA
CACCGTACTTTCTATGAGAAGCGTA	This paper	For-RPS6-sgRNA-2
AAACTACGCTTCTCATAGAAAGTAC	This paper	Rev-RPS6-sgRNA-2
Recombinant DNA		
pCDH1-ATF4-tGFP-Blasticidin	Bartok et al. (2021)	N/A
pCDH1-ATF4-tGFP-SIINFEKL-Blasticidin	Bartok et al. (2021)	N/A
pCDH1-ATF4+1-tGFP-Blasticidin	Bartok et al. (2021)	N/A
pCDH1-ATF4+1-tGFP-SIINFEKL-Blasticidin	Bartok et al. (2021)	N/A
pCDH1-H2Kb-Hygromycin	This paper	N/A
pCMV(CAT)T7-SB100	Gift from Z.Izsvak	Addgene plasmid 34879
pLentiCRISPRv2 puro	Addgene	Addgene plasmid 98290
pLKO.1-tGFP plasmid	Gift from Dr. Beijersbergen	N/A
pSBbi-pur H-2Kb	Gift from J. Yewdell	Addgene plasmid 111623
Software and algorithms		
Adobe Illustrator CC 2017	Adobe acrobat	https://www.adobe.com
Adobe Photoshop CC 2017	Adobe acrobat	https://www.adobe.com
FlowJo V10 software (FlowJo)	FlowJo	https://www.flowjo.com/
TraceFinder software	Thermo Fisher Scientific	https://www.thermofisher.com/us/en/home.html
Prism7	GraphPad software	https://www.graphpad.com/scientific-software/prism/

RESOURCE AVAILABILITY

Lead contact

Further information and requests for resources and reagents should be directed to and will be fulfilled by the lead contact, Reuven Agami (r.agami@nki.nl).

Materials availability

All unique materials and reagents generated in this study are available from the lead contact with a completed material transfer agreement.

Data and code availability

Processed data generated for proteomics (related to Figure 1D) in this study are available in the PRIDE repository with accession code PXD022707 (Perez-Riverol et al., 2019).

Original western blot images have been deposited at Mendeley and are publicly available as of the date of publication: https://doi.org/10.17632/fxws8gn867.1.

Any additional information required to re-analyze data reported in the paper is available from the lead contact upon request.

EXPERIMENTAL MODEL AND SUBJECT DETAILS

Mice

Intestinal organoids were derived from VillinCre^{Ert2} and VillinCre^{Ert2} APC$^{fl/fl}$ KRAS$^{G12D/+}$ C57BL/6J mice, aged 8-12 weeks without any gender selection. Cre recombinase was induced *in vivo* by injecting tamoxifen (80mg/kg). 3 days later, mice were sacrificed and the crypts were extracted.

Crypt isolation and organoid culture

Murine intestinal crypts were isolated from VillinCre^{Ert2} and VillinCre^{Ert2} APC$^{fl/fl}$ KRAS$^{G12D/+}$ mice and maintained, as described previously (van Es and Clevers, 2015). Briefly, small intestines were isolated, opened longitudinally, scraped to remove the villi and washed with ice-cold PBS. The tissue was chopped into 5mm pieces and washed several times with ice-cold PBS. The intestinal pieces were then incubated with cold 2mM EDTA for 30 minutes and then washed with ice-cold PBS several times. The 2nd, 3rd and 4th washes were collected (crypt enriched fractions). Crypt fractions were combined, pelleted down, resuspended in Advanced DMEM/F12 (Thermo Fisher Scientific) and passed through a 70-μm strained. The crypts were washed a couple of times in Advanced DMEM/F12 and then casted into 30μl Cultrex Reduced Growth Factor Basement Membrane Extract (BME, R&D System) plugs and cultured in complete medium (advanced DMEM/F12 supplemented with 10mM HEPES, 1X Glutamax, 100 U/mL penicillin/streptomycin, 2% B-27 supplement (Thermo Fisher Scientific), 1% N-2 supplement (Thermo Fisher Scientific) and 0,8% BSA supplemented with 10% Noggin conditioned medium, 50ng/ml EGF (Peprotech) and, for the WT organoids, also 10% R-spondin conditioned medium (Peprotech).

Cell culture

Excepted for BJ-EHT, D10, MD55A3, TIG-3 and 108T, all cancer cell lines originated from the American Tissue Culture Collection (ATCC) and grown in the recommended culture media.

In details, A-375, 108T, SK-MEL-28, MDA-MB-231, MCF-7, MDA-MB-468, BT-474, A549, HT-29, HCT 116, SK-OV-3, MIA Paca-2, U-2 OS, SW1573, WiDR, SW480, LS174T and U-87 MG were cultured in Dulbecco's modified Eagle's medium (DMEM; GIBCO), supplemented with 10% fetal bovine serum (Sigma) and 100 U/ml penicillin–streptomycin (GIBCO).

D10, T-47D, ZR-75-1, BT-459, HCC827, NCI-H1299, NCI-H358, OVCAR-3, OVCAR-4, Capan-1, Aspc-1 and PC-3 were maintained in Roswell Park Memorial Institute 1640 Medium (RPMI 1640, GIBCO) supplemented with 10% fetal bovine serum (Sigma) and 100 U/ml penicillin–streptomycin (GIBCO).

A375DR (NRASQ61H) were cultured in Dulbecco's modified Eagle's medium (DMEM; GIBCO), supplemented with 10% fetal bovine serum, 100 U/ml penicillin–streptomycin and under pressure of 2μM PLX4032 (MedKoo).

MD55A-3 was derived from metastatic melanoma tumor resections (Bartok et al., 2021) and were maintained in Roswell Park Memorial Institute 1640 Medium (RPMI 1640, GIBCO) supplemented with heat-inactivated 10% fetal bovine serum (Sigma), 25 mM HEPES (GIBCO) and 100 U/ml penicillin–streptomycin (GIBCO). MCF 10A were also purchased from ATCC and were cultured in DMEM/F-12, HEPES medium (Thermo-Fisher scientific) supplemented with 5% horse serum (Thermo-Fisher scientific), EGF (10 ng/ml; Millipore), insulin (10 μg/ml; Sigma), and hydrocortisone (500 ng/ml; Sigma).

HEK293T, hTERT-RPE1, BJ/ET and TIG3/ET were cultured in Dulbecco's modified Eagle's medium (DMEM; GIBCO), supplemented with 10% fetal bovine serum and 100 U/ml penicillin–streptomycin. For BJ-EHT/P53KD/iHRAS^{G12V}, HRAS expression was induced by treating the cells 7 days with 4-OH-tamoxifen (4-OHT; Sigma) (Voorhoeve et al., 2006).

All cell lines were maintained in a humidified atmosphere containing 5% CO2 at 37 °C, tested regularly and were found negative for mycoplasma contamination (EZ-PCR mycoplasma kit; Biological Industries).

Tryptophan-free DMEM/F-12 medium was purchased from US Biologicals, custom-made tyrosine-free medium was purchased from Cell Culture Technologies and IFNγ (PeproTech) was used at 250 U/ml for 48 h. MG-132 (Selleckchem), dissolved in DMSO, was used at a final concentration of 10 μM. IDO inhibitors; 1-methyl-L-tryptophan (Sigma) was dissolved in 0.1M NaOH at a 20 mM concentration adjusted to pH 7.5, filter-sterilized and used at a final concentration of 300 μM for 48 h; Epacadostat (Selleckchem) was diluted in DMSO and used for 48h at 200nM. Polyethylenimine (PEI, Polysciences) was dissolved in water at a concentration of 1 mg/ml, after which it was filter-sterilized, aliquoted and stored at −20 °C.

OT-1 T cells isolation and culture

OT-I T cells were isolated using DynabeadsTM UntouchedTM Mouse CD8 Cells Kit (Invitrogen) according to manufacturer's protocol. T cells were initially maintained in Roswell Park Memorial Institute 1640 Medium (RPMI 1640, GIBCO) containing 10% fetal calf serum (FCS), 50μM 2-Mercaptoethanol (Sigma), 100U/mL of penicillin, 100 μg/ml of streptomycin, 10ng/mL IL-2 (Proleukin, Novartis), 0,5ng/mL IL-7 (ImmunoTools) and 1ng/mL IL-15 (ImmunoTools).

METHOD DETAILS

Cell treatments

For all the experiments of this manuscript, cells were seeded 1 day before the experiment. Then for 48 h cells were exposed to IFNγ (250U/mL, Peptrotech), or to Tyrosine depleted medium (Cell culture Technologies) or to Tryptophan depleted medium (US Biological

Life Sciences). At the same time of IFNγ, IDO-1 inhibitor was also used when mentioned (1-Methyl-L-tryptophan, 300 μM or Epacadostat, 200nM).

24 h after the beginning of the treatment, as mentioned in each figures, the drugs of interest were added: PLX4032 (MedKoo), Trametinib (Selleckchem), Gefetinib (Selleckchem), Torin-1 (Selleckchem), LJH685 (RSP6KAi, Selleckchem), Nocodazole (Selleckchem), Nutlin-3A (Gift from W. Zwart). Only for Western Blot analysis, after those 48 h, cells were treated for an additional 4 h with proteasome inhibitor (MG-132, 10 μM, Selleckchem).

For tryptophan depletion experiment using mice organoids, organoids were casted into 30μl BME plugs (5 plugs per condition) and cultured in complete medium supplemented with growth factors Noggin, EGF and, for WT organoids, also R-spondin as already described above. After 2 days in culture, the media was replaced by either DMEM/F-12 media with or without Tryptophan, supplemented with recombinant Noggin 100ng/ml (Peprotech), 50ng/ml EGF (Peprotech) and, for WT organoids, recombinant R-spondin 500ng/ml (Peprotech) as well. After 48 h in culture, proteasome inhibitor MG-132 (10 μM) was added for 4 h and then the organoids were collected.

Cloning

V5-ATF4$^{(1-63)}$-tGFP and V5-ATF4$^{(1-63)}$ +1-tGFP were generated by PCR. A first PCR product was generated by amplifying V5-ATF4 using the primers listed in the STAR Methods section. This PCR product was then extended with turbo-GFP (from pLKO.1-tGFP plasmid) by a 2nd PCR with the V5-ATF4$^{(1-63)}$-tGFP or V5-ATF4$^{(1-63)}$ +1-tGFP plasmid as a template. The V5-ATF4$^{(1-63)}$-tGFP and V5-ATF4$^{(1-63)}$ +1-tGFP gene were then inserted in the pCDH-Blast or pCDH-Puro vector by restriction/ligation cloning in the XbaI and NotI sites.

A DNA sequence coding for the amino acid sequence LEQLESIINFEKL was cloned immediately downstream of the tGFP sequence by PCR in the pCDH-V5-ATF4$^{(1-63)}$-tGFP and pCDH-V5-ATF4$^{(1-63)}$-+1-tGFP reporter constructs. The resulting PCR products were then inserted by restriction/ligation cloning in the XbaI and NotI sites in the pCDH-Blast or pCDH-Puro vector.

The H2-K^{b} gene was amplified from cDNA using the primers listed in the STAR Methods section. The PCR product was cloned into pCDH-puro backbone by restriction/ligation cloning by making use of the XbaI and EcoRI sites. Next, the puromycin selection cassette was replaced by a hygromycin cassette. This cassette and the PGK promoter were amplified by PCR using the primers in the STAR Methods section and the pLenti-Hygro plasmid as a template. The resulting DNA fragment was introduced between the BamHI and XhoI sites of the pCDH-H2-Kb plasmid by a restriction/ligation procedure.

For Crispr-Cas9 cloning, pLenti-CRISPR-V2 plasmid was digested using BsmBI and FastAP enzymes. Then the digested vector was purified using Gel purified kit (Promega). In the meantime, oligonucleotides against RPS6 (listed in STAR Methods) were annealed and phosphorylated using T4 PNK. The digested vector and the annealed product were ligated using T4 DNA Ligase. Finally, the reaction product was used to transform DH5α-bacteria.

All resulting plasmids were sequence verified by Sanger sequencing (Macrogen).

Lentiviral production and transduction

For lentivirus production, 3.5 × 10^{6} HEK293T cells were seeded per 10cm dish, one day prior to transfection. For each transfection, 10 μg of the pCDH vector of interest, 5 μg of pMDL RRE, 3.5 μg pVSV-G and 2.5 μg of pRSV-REV plasmids were mixed in 500 μL of serum- free DMEM. Next, 500 μL of serum-free DMEM containing 63 μL of a 1 mg/mL PEI solution was added. The entire mix was vortexed and left for 20 min at room temperature after which it was added to the HEK293T cells to be transfected. The next day, the medium was refreshed and the lentivirus-containing supernatants were collected 48 and 72 h post transfection, and snap frozen in liquid nitrogen. Target cells were transduced by supplementation of the lentiviral supernatant with 8 μg/mL polybrene. 24 h later, transduced cells were selected by addition of 5 μg/mL blasticidin (Invivogen), 2 μg/mL puromycin (Bio-connect) or a range of 50-200 μg/mL hygromycin B (GIBCO) to the medium.

In regard to organoids infection, virus supernatant was collected, filtered through a 0,45μm filter and concentrated by adding 1 volume of LentiX Concentrator (Takara) to 3 volumes of supernatant and incubating for 4 h at 4°C. The solution was centrifuged for 45min at 1500 g at 4°C and pellets resuspended in ice-cold PBS.

Viral transduction of intestinal organoids

Transfection of organoids was performed based on a previously described protocol (Maru et al., 2016). Briefly, organoids were cultured in complete medium with growth factors (Noggin, EGF and, for WT organoids, R-spondin as well) and stem cell-inducing factors: 10μM Rho kinase inhibitor Y-27632 (Cayman) and 1mM VPA (Biovision). For WT organoids were also added 1μM Jagged-1 (AnaSpec) and 6μM CHIR99021 (Cayman). After 2 days in culture, organoids were then collected and mechanically dispersed by pipetting several times, followed by incubation with accutase (Thermo Fisher Scientific) to obtain single cells. After washing, cells were resuspended in complete medium, containing growth factors, stem-cell inducing factors and 8μg/ml polybrene. The cell mix was laid over wells covered with a thin layer of BME. The virus was added to each well and incubated in normal culture conditions (37°C 5% CO2) for 24 h. The media was then removed, a thin layer of BME was put on top of the organoids and the organoids were cultured in complete medium, containing growth factors and stem-cell inducing factors, for another day. 48 h post-infection, selection of the infected organoids with blasticidin (Invivogen, 6μg/ml for WT and 10μg/ml for APC$^{-/-}$KRAS^{G12D} organoids) started.

Amino acid mass spectrometry

Two days after IFN stimulation or relevant amino acid depletion, cells were washed with cold PBS and lysed with lysis buffer composed of methanol/acetonitrile/H2O (2:2:1). The lysates were collected and centrifuged at 16,000 g (4°C) for 15 minutes and the supernatant was transferred to a new tube for liquid-chromatography mass spectrometry (LC-MS) analysis.

LC-MS analysis was performed on an Exactive mass spectrometer (Thermo Scientific) coupled to a Dionex Ultimate 3000 autosampler and pump (Thermo Scientific). Metabolites were separated using a Sequant ZIC-pHILIC column (2.1 × 150 mm, 5 μm, guard column 2.1 × 20 mm, 5 μm; Merck) using a linear gradient of acetonitrile (A) and eluent B (20 mM (NH4)2CO3, 0.1% NH4OH in ULC/MS grade water (Biosolve), with a flow rate of 150 μL/min. The MS operated in polarity-switching mode with spray voltages of 4.5 kV and −3.5 kV. Metabolites were identified on the basis of exact mass within 5 ppm and further validated by concordance with retention times of standards. Quantification was based on peak area using TraceFinder software (Thermo Scientific).

Analysis of IP-based mass spectrometry data

(a) Data generation

At the end of each experiment intended for V5-tag pulldown, cells were treated with 10 μM MG-132 for 4 h and subsequently collected by trypsinization and centrifugation. Next, cells were lysed in 300 μL ELB lysis buffer (50 mM HEPES, 125 mM NaCl, 0.5% (v/v) Tween-20 and 0.1% (v/v) Nonidet P40 Substitute). Next, 3μL of mouse anti-V5 antibody solution (1.0 mg/mL, Invitrogen) was added to the lysate and the samples were incubated on a rotating wheel at 4°C overnight. Pulldowns were performed with Dynabeads protein G (Invitrogen) according to manufacturer's protocol. All pulled down protein was eluted in 30 μL of 1x Laemmli buffer.

Next, the eluates were run briefly into a 4%–12% Criterion XT Bis-Tris gel (Bio-Rad) and short, Coomassie-stained gel lanes were excised for each sample. Proteins were reduced with 6.5mM DTT, alkylated with 54mM iodoacetamide and digested in-gel with trypsin (Gold, mass spectrometry grade, Promega, 3ng/μL) overnight at 37°C. Extracted peptides were vacuum dried, reconstituted in 10% formic acid and analyzed by nanoLC-MS/MS on an Orbitrap Fusion Tribrid mass spectrometer equipped with a Proxeon nLC1000 system. Peptides were loaded directly on the analytical column and separated in a 90-minutes gradient containing a non-linear increase from 5% to 26% solvent B.

(b) Generation of search database (DB)

One search DB was generated. This DB consisted of the original ATF4 in-frame protein sequence, the ATF4 sequence until W93 and frameshifted (+1) at W-codon until the first stop codon (Figure 1A).

(c) Searching of IP-mass-spec data against the DBs

The search was performed using MaxQuant (version 1.6.0.16) (Tyanova et al., 2016). The parameters of the search were optimized for increasing sensitivity and is deposited in the PRIDE DB (Perez-Riverol et al., 2019).

Western blotting

Straight lysates from cells were made in 6 wells by addition of 200 μL of 1x Laemmli buffer without 2-mercaptoethanol and bromophenol blue. Samples were boiled and protein content was assessed by performing BCA protein quantification (Thermofisher). Then, 2-mercaptoethanol and bromophenol blue were added and the same amount of protein per samples (between 15-30 μg) was loaded and run on SDS-PAGE gels and blotted on 22 μm pore size nitrocellulose membranes (Santa Cruz). Then, membranes were stained with the appropriate antibodies (see the reference list in the STAR Methods).

Subsequent staining were performed with the appropriate LI-COR secondary antibodies (see the list in the STAR Methods). Visualization was performed by use of an Odyssey infrared scanning device (LI-COR).

For all the Western Blot assessing frameshifting, a *sloppiness* index is displayed next to the figure. This index is calculated for the cell lines expressing the pSloppy^{FS} reporter by dividing the intensity of the frameshifting band (#) by the *in-frame* product (&) from the V5 staining. Note that for the Figure 1F the background signal obtained from this quantification in the basal condition (+W) was subtracted to the ratio obtained in the -W condition.

qPCR analyses

Total RNA was isolated using Trizol reagent (Thermo Fisher Scientific) following the manufacturer's instructions. Briefly, cells were washed with PBS and 500 μL Trizol was added for harvesting the cells. After mixing with chloroform (Sigma Aldrich) and centrifuge, the aqueous phase was transferred to a new tube and mixed with 2-Propanol (Sigma Aldrich) for RNA precipitation by centrifuging at 4°C for 30 min. RNA pellet was washed with 70% ethanol and finally dissolved in RNase-free water (Life technologies).

Reverse transcription was performed with Tetro Reverse Transcriptase kit (Bioline) according to the manufacturer's instructions using 1 μg of total RNA per reaction. qPCR products were prepared using a SensiFAST SYBR No-ROX kit (Bioline) according to the instructions and performed in the Light Cycler 480 (Roche). Primers used are listed in the STAR Methods.

Flow cytometry (SIINFEKL assays)

MD55A3, A-375 and A-375DR cells were transduced with pCDH-Hygro-H2-Kb and selected. Next, the H-2-Kb expressing cells were transduced with lentiviruses generated from the pCDH-V5-ATF4$^{(1-63)}$-tGFP-SIINFEKL (frame or +1) constructs, after which they were selected with blasticidin or puromycin accordingly.

For the detection of presented H2-Kb-bound SIINFEKL peptides, cells were treated for 48 h with IFNγ and the last 24 h with the indicated drugs (see the section Cell treatments). Then, cells were washed with PBS and detached using 300 μL PBS-EDTA for a 6 wells plate. Next, cells were pelleted and washed with PBS-BSA (0.5%) and incubated with APC anti-mouse H-2Kb-bound to SIINFEKL antibodies (Biolegend, clone 25-D1.16, #141606; 1:200) for 30 minutes on ice and in the dark. Next, the cells were washed two times with PBS-BSA (0.1%) and analyzed on an Attune NxT machine (Thermo Fisher Scientific). Data were analyzed using FlowJo V10 software (FlowJo). For some experiments using drugs, cells were resuspended with PBS-BSA (0.1%) supplemented with DAPI (0.2 μg/mL; Thermo Fisher Scientific).

Detection of T cell reactivity

A-375 and A-375DR cells expressing H2-Kb and V5-ATF4$^{(1-63)}$-tGFP-SIINFEKL or V5-ATF4$^{(1-63)}$-+1-tGFP-SIINFEKL were treated for 48 h with IFNγ and with IDO1 inhibitor (300 μM) or the last 24 h with PLX4032 (500nM, Medkoo). To the IFNγ-treated samples, 7.2 × 10^2μg/mL purified PEG-HIS-mpKynureninase (Triplett et al., 2018) and 2 μM pyridoxal 5′-phosphate hydrate (Sigma) were added. At the end of the treatment, cells were detached using PBS-EDTA and seeded at 100,000 cells per well in a U-shaped 96 well plate. Next, 100,000 OT-I T cells were added to start the co-culture and the solution was supplemented with BD Golgi-plug (BD Biosciences). The co-culture samples were then incubated for 12 h at 37°C in a humidified CO2 incubator.

Next, the cells were pelleted by centrifugation, blocked with 0.1% PBS-BSA and stained with anti-mouse CD8-VioBlue antibodies (Miltenyi, #130-111-638) and Live/Dead Fixable near-IR dead cell stain kit (Invitrogen). Subsequently, the cells were fixed and permeabilized using the eBioscienceTM Foxp3 Transcription Factor Staining Buffer Set (Invitrogen) according to manufacturer's instructions. Next, the cells were stained with APC-conjugated anti-mouse IFNγ (Miltenyi, #130-109-723) and PE-conjugated anti-mouse TNFα (Miltenyi, #130-109-719) antibodies. Cells were then washed and analyzed on a BD LSR Fortessa (BD Biosciences). The data were analyzed using FlowJo V10 software (FlowJo).

T cell killing assay and clonogenic assay

A-375 and A-375DR cells expressing H2-Kb and V5-ATF4$^{(1-63)}$-+1-tGFP-SIINFEKL were treated for 48 h with IFNγ and with IDO1 inhibitor (1-methyl-L-tryptophan 300 μM; epacadostat 200nM) or the last 24 h with PLX4032 (500nM, Medkoo). To the IFNγ-treated samples, 7.2 × 10^2μg/mL purified PEG-HIS-mpKynureninase (Triplett et al., 2018) and 2 μM pyridoxal 5′-phosphate hydrate (Sigma) were added. After these initial 48 h, cells were refreshed with DMEM media supplemented with Kynureninase and IDOi for the corresponding samples. Then OT-1 cells were added for another 24 to 48 h to the co-culture. Different concentrations of OT-1 cells were used starting from 5 times less than cancer cell (1:5) to 5 times more (5:1). The best ratio is displayed in the figures. After 1 or 2 day of co-culture, cells were refreshed, rinsed with PBS and fixed for 30min at RT with 4% formaldehyde. Then cells were stained using Crystal Violet (0,1%) for 1hr at RT in the dark. Then wells were thoroughly washed with water and dried overnight. To quantify killing efficiency, wells were unstained using a 10% acetic acid solution and measured at 590nM using a TECAN.

QUANTIFICATION AND STATISTICAL ANALYSIS

Quantification of the band intensity was done using ImageJ. The sloppiness index calculated from this quantification is explained in the section Western blotting.

One way-ANOVA followed by Bonferroni or Sidak post hoc test was used for all statistics analysis used in the paper. Prism 7 software was used for all statistical analyses and for data visualization. Statistical details about n number and p value are reported in Figure legends.